UNIVERSITÉ DU QUÉBEC À MONTRÉAL

EXTRÊMES CLIMATIQUES EN ZAMBIE LORS DES PÉRIODES DE SAHARA VERT ET HUMIDE ET IMPACTS SUR LA DISPERSION ET L'ÉVOLUTION DES HUMAINS

MÉMOIRE

PRÉSENTÉ

COMME EXIGENCE PARTIELLE

DE LA MAÎTRISE EN SCIENCES DE L'ATMOSPHÈRE

PAR

DOMINIC ALAIN

NOVEMBRE 2023

UNIVERSITÉ DU QUÉBEC À MONTRÉAL
Service des bibliothèques

Avertissement

REMERCIEMENTS

TABLE DES MATIÈRES

iv

LISTE DES FIGURES

LISTE DES TABLEAUX

LISTE DES ABRÉVIATIONS, DES SIGLES ET DES ACRONYMES

AHP   Période Humide Africaine (African Humid Period)

ASS/SSA   Afrique subsaharienne (Sub-Saharan Africa)

AP/BP   Avant le présent (Before Present)

CLASS   Canadian LAnd Surface Scheme

CMC   Centre météorologique canadien

CAP   Central African Plateau

CDD   Consecutive dry days

MRCC5/CRCM5   5e génération du modèle régional canadien du climat (Canadian Regional Climate Model version 5)

GCM   Modèle climatique global (Global Climate Model)

ZCIT/ITCZ   Zone de convergence intertropicale (Intertropical Convergence Zone)

HM/MH   Holocène moyen (Mid-Holocene)

ISBA   Interaction Sol-Biosphère-Atmosphère

LI$_{DS}$ Basse Insolation Sahara sec (Low Insolation Dry Sahara)

LI$_{GS}$ Basse Insolation Sahara humide (Low Insolation Green Sahara)

HI$_{GS}$	Haute Insolation Sahara humide (High Insolation Green Sahara)
NE	Northeast
NOAA	National Oceanic and Atmospheric Administration's National Climatic Data Center
PI	Préindustriel (Pre-Industrial)
PMIP	Paleoclimate Model Intercomparison Project
RPN	Recherche Prévision Numérique
RR	Taux de précipitation (Rain Rate)
SPI	Standardized Precipitation Index
STI	Standardized Temperature Index
SW	Southwest
MRC/RCM	Modèle régional de climat (Regional Climate Model)
MOA/WAM	Mousson ouest africaine (West African Monsoon)

RÉSUMÉ

Le nord de l'Afrique a traversé des périodes humides connues sous le nom de périodes humides africaines ou périodes pluviales du Sahara au courant du Pléistocène tardif et de l'Holocène qui auraient pu avoir un impact sur la dispersion des humains à travers l'Afrique. Cependant, peu est connu à propos des changements sur les extrêmes climatiques dans le Centre-Sud de l'Afrique, associés à ces cycles et leurs impacts potentiels sur le déplacement des humains. Dans cette étude, nous utilisons un modèle climatique régional afin de simuler des périodes archétypes du Sahara vert, ainsi que désertique, sous des conditions d'insolation estivale boréale élevée et faible, et étudions les impacts résultant des changements climatiques et leurs extrêmes en Afrique centrale et australe, notamment dans la région centrale, la Zambie. Nos résultats indiquent des conditions plus chaudes et sèches sous les conditions du Sahara vert par rapport aux périodes du Sahara désertique. Plus précisément, les périodes de sécheresse sont allongées, et les températures extrêmes simulées sont plus chaudes en Zambie dans la simulation du Sahara vert. Nos résultats suggèrent que lors des périodes du Sahara désertique, la Zambie aurait possiblement offert de meilleures conditions environnementales pour les hominidés dans le grand plateau centrafricain. En revanche, les périodes du Sahara vert ont offert les conditions inverses, forçant potentiellement les populations d'hominidés de se disperser à travers les grandes vallées vers le plateau centrafricain ainsi que vers le nord via le Sahel et le Sahara.

Mots-clés : Sahara vert, Zambie, extrêmes climatiques, dispersion des humains, Holocène moyen.

INTRODUCTION

Des preuves archéologiques et paléontologiques récentes suggèrent une origine panafricaine complexe pour notre espèce, *Homo sapiens*, dans lesquelles l'Afrique subsaharienne (ASS) a joué un rôle majeur (Hublin *et coll.*, 2017 ; Scerri, 2017; Stringer & Galway-Witham, 2017 ; Klein & Richard Klein, 2019 ; Wilkins, 2021). Il est cru que la variabilité climatique antérieure en ASS, plus particulièrement en Afrique tropicale du Sud, peut avoir influencé la dynamique des populations humaines et leur évolution à l'échelle du continent africain (Blome *et coll.*, 2012 ; John E. Kutzbach *et coll.*, 2020). Elle influe également le développement socioéconomique contemporain de cette région, par exemple la sécurité alimentaire et les conditions d'hébergement décentes. L'accès à l'eau potable y est une importante contrainte, nous imposant comme objectif le besoin de préserver cette ressource dans un endroit où l'agriculture pluviale domine (IFAD, 2013). Il est donc impératif d'identifier les facteurs qui contrôlent le développement du réseau hydrologique et les cycles climatiques qui les influencent.

L'ASS est dominée par un plateau central de plus de 1 million de km^2, qui s'étend du rift africain jusqu'à la zone tropicale humide (Daly *et coll.*, 2020). Le plateau est drainé par le Zambèze, le troisième plus grand réseau hydrologique du continent africain. Ce système de drainage, qui passe par la Zambie avant de s'écouler dans l'océan indien, est considéré par les archéologues d'être un important corridor biogéographique, influençant potentiellement le comportement des occupations d'hominidés dans la région pendant l'âge de la pierre avec de potentielles répercussions sur l'évolution humaine. (Larry Barham, 2000 ; Burrough *et coll.*, 2019 ; Colton *et coll.*, 2021).

La région ASS est située dans les tropiques, elle a ainsi un climat de moussons avec une grande variabilité de précipitation annuelle et interannuelle (Mason *et coll*., 1997 ; Richard *et coll.*, 2001; Fauchereau *et coll.*, 2003) d'où l'importance de comprendre les facteurs pouvant avoir une incidence sur cette variabilité. Les moussons sont un déterminant majeur des climats tropicaux régionaux. Sur des échelles de temps annuelles et interannuelles, trois différents flux d'humidité de surface influencent les régimes de pluie dans l'ASS, particulièrement dans le Centre-Sud de l'Afrique (Torrance, 1972 ; Nicholson, 1996). Le déplacement méridional de la zone de convergence intertropicale (ZCIT) conduit l'humidité, qui provient initialement de la mousson sud-est de l'Afrique durant la saison humide, une période de pluie abondante de novembre à avril, avec un pic de précipitation de décembre à février. Le « Congo Air Boundary » divise les vents d'alizés soufflant de l'est des vents saisonniers de la mousson, permettant la rencontre du flux d'humidité provenant de l'Atlantique, et du flux provenant de l'océan indien (Nicholson, 2002). Cependant, la durée des saisons sèches et humides de la mousson ouest-africaine démontre des variations significatives d'échelles de temps allant d'interannuelle, décennale et plus longue. Par exemple, une période de pluie abondante s'est abattue sur le Centre-Sud de l'Afrique en janvier 2013 et a mené à des inondations avec des journées de pluie enregistrées dépassant les 200 millimètres sur une période de dix jours dans quelques régions (Manhique *et coll*., 2015). Par ailleurs, une grave sècheresse a touché le sud de l'Afrique en 1991-1992 et a mené à une baisse dans la production de cultures et de réserves alimentaires (Vogel & Drummond, 1993).

Le continent africain a subi plusieurs dérives climatiques depuis le Miocène tardif (il y a ~11,6 à 5,3 ma), l'évènement le plus notable étant les périodes humides africaines, au cours desquelles les moussons africaines se sont intensifiées et la ZCIT s'est déplacée vers le nord, transformant les zones arides, tel que le Sahara, en habitats mésiques (Gasse, *et coll.*, 1990 ; deMenocal & Tierney, 2012).

Les périodes humides africaines

Plusieurs archives paléoclimatiques ont démontré que le nord de l'Afrique a connu d'intenses phases sèches et humides. Le désert du Sahara actuel et le Sahel (zone de transition entre le Sahara et les forêts tropicales africaines) ont jadis été des zones contenant davantage de végétation avec un mélange de forêts et de prairies, et des lacs (Yu & Harrison, 1996 ; Gasse, 2000 ; Castañeda *et coll*., 2009). Les archives paléoclimatiques disponibles témoignent de l'existence de cycles humides et arides (Hoelzmann *et coll*., 1998 ; deMenocal *et coll*., 2000 ; Hély *et coll.*, 2014 ; Tierney *et coll.*, 2017), et nous indiquent que l'oscillation entre un Sahara sec et un Sahara humide a eu lieu depuis le Miocène tardif (Larrasoaña *et coll*., 2013 ; deMenocal *et coll*., 1995 ; Drake *et coll*., 2008). La plus récente de ces périodes humides africaines est survenue au cours de l'Holocène entre 11 000 et 5 000 ans avant le présent (A.P.). L'existence de paléolacs et des assemblages de pollen de végétation de type savane sont quelques exemples de données qui démontrent la présence d'un Sahara humide et vert par le passé.

La période humide africaine résulte de l'influence de la géométrie orbitale de la Terre (précession) sur la mousson (Berger, 1978). Quand la Terre est davantage rapprochée du Soleil pendant l'été boréal et plus éloignée durant l'hiver boréal par rapport à l'actuel, les étés plus chauds dans l'hémisphère nord augmentent le contraste thermique terre-mer, causant une progression vers le nord de la circulation de Hadley. Cela permet à la mousson ouest-africaine de pénétrer davantage vers le nord du continent africain (Kutzbach, 1981 ; Gaetani *et coll*., 2017). On assiste alors à une augmentation drastique de la précipitation dans la région saharienne, à un verdissement dans le désert du Sahara et à une migration de la végétation sahélienne qui atteint 28-30° N (Hély *et coll*., 2014). Au total, 230 périodes humides africaines ont été identifiées depuis le Miocène, soulevant la question ; comment la variabilité climatique de la région saharienne

africaine a-t-elle pu influencer l'évolution et la dispersion des hominines au cours du Pléistocène à l'échelle panafricaine (Larrasoaña *et coll.*, 2013) ?

Plusieurs études antérieures suggèrent que les corridors pluviaux créés dans la région saharienne pendant les périodes humides africaines pourraient avoir favorisé la dispersion des hominines (Szabo *et coll.*, 1995 ; Osborne *et coll.*, 2008 ; Castañeda *et coll.*, 2009 ; Drake *et coll.*, 2011 ; Smith, 2012, Hublin *et coll.*, 2017). Plus récemment, des chercheurs ont proposé que l'évolution de notre espèce, *Homo sapiens*, ait pu se dérouler à l'échelle continentale suite aux cycles climatiques favorisant les contacts entre les populations dans le « berceau de l'humanité », en Afrique du Sud, et les populations hominines ailleurs en Afrique, notamment en Afrique du Nord (Hublin *et coll.*, 2017 ; Richter *et coll.*, 2017). Cependant, les routes exactes utilisées et le modèle de dispersion au sein de l'Afrique sont méconnus (Agustí & Lordkipanidze, 2011 ; Abbate & Sagri, 2012 ; Reynolds, 2015, Timmermann & Friedrich, 2016). Une dynamique similaire est suggérée pour la zone tropicale sud de l'Afrique, où le plateau central et le désert du Kalahari ont alterné entre des conditions arides et relativement humides, limitant potentiellement la distribution des populations d'hominidés, et renforçant l'importance des cours d'eau importants, par exemple le Zambèze comme un potentiel refuge (Burrough *et coll.*, 2019). Le rôle de la variabilité climatique sur l'évolution des hominidés est reconnu depuis le début des recherches paléoanthropologiques puisque cela affecte la distribution des habitats favorables pour la survie humaine (deMenocal, 2004 ; Potts et Faith, 2015).

Des études récentes ont souligné de quelle façon le renforcement de la mousson ouest-africaine peut influencer le climat de régions éloignées, et ce, par la suppression d'El Niño (Pausata *et coll.*, 2017a), une augmentation dans le taux de précipitation des moussons dans l'hémisphère nord (Sun *et coll.*, 2019), un décalage vers le nord de la mousson asiatique (Piao *et coll.*, 2020), ou des changements dans l'activité tropicale cyclonique (Pausata *et coll.*, 2017b). Jusqu'à maintenant, peu d'études ont examiné

l'impact du verdissement du Sahara en combinant la précession, la couverture végétale et la réduction de poussière atmosphérique, et en étudiant leur impact sur le climat dans des régions éloignées, telle la zone sud-tropicale de l'Afrique et plus particulièrement en Zambie.

Le but ultime de cette étude est donc d'analyser les changements climatiques associés aux périodes humides et sèches du Sahara dans l'ASS, plus particulièrement les changements dans les évènements extrêmes de température et de précipitation en Zambie, qui occupe une place centrale dans la zone sud-tropicale de l'ASS.

Le présent mémoire est structuré comme suit : le chapitre 1 présente un article scientifique rédigé en anglais. La description du modèle, le lieu d'étude et son climat, la conception expérimentale et les indices climatiques extrêmes sont abordés dans la section 2. Les résultats sont présentés dans la section 3 qui est divisée en sous-sections : 1) changements dans la température moyenne annuelle et saisonnière, 2) changements dans la précipitation moyenne annuelle et saisonnière, 3) changements dans les indices extrêmes de température, 4) changements dans les indices extrêmes de précipitation et 5) changements dans les cycles saisonniers annuels moyens de température et de précipitation. Finalement, une discussion des retombées pour notre compréhension du modèle d'évolution de notre lignée, ainsi que la compréhension des variables clés influençant l'hydrologie du secteur et son potentiel économique se retrouvent à la section 4. La section 5 comprend les figures, annexes ainsi que la bibliographie et complète le mémoire.

CHAPITRE I

EXTRÊMES CLIMATIQUES EN ZAMBIE ENTRE LES PÉRIODES DE SAHARA
VERT ET HUMIDE ET IMPACTS SUR LA DISPERSION DES HUMAINS

Ce chapitre est composé d'un article scientifique rédigé en quatre différentes sections. La section 1 inclut l'introduction au sujet. La méthode utilisée pour l'analyse des résultats est présentée dans la section 2 de l'article. La section 3 dévoile l'ensemble des résultats de la recherche ainsi que leur analyse. Pour conclure, la section 4 discute des résultats et en fait la synthèse.

Changes in Climate extremes in Zambia during Green and Dry Sahara periods and their potential impacts on hominid dispersal

Dominic ALAIN, Francesco S.R. PAUSATA, Roberto INGROSSO,, Katja WINGER, Michelle S.M. DRAPEAU and Ariane BURKE

Centre ESCER (Étude et la Simulation du Climat à l'Échelle Régionale) and GEOTOP (Research Center on the dynamics of the Earth System), Department of Earth and Atmospheric Sciences, Université du Québec à Montréal, Montréal

Department of Anthropology, Université de Montréal, Montréal

ABSTRACT

Northern Africa experienced humid periods known as African humid periods or Green Sahara periods during the late Pleistocene and Holocene. The waxing and waning of the African Monsoon over the last several million years raises the question of how the climatic variability in the African Saharan region could have influenced the evolution and dispersion of hominins in Africa. Little is yet known about the changes in climate extremes in central southern Africa associated with these cycles and their potential impacts on human migration. In this study, we use a regional climate model to simulate archetypal Green and Desert Sahara periods under high and low boreal summer insolation and investigate the resulting changes in climate variability and extremes in South Tropical Africa, with a focus on Zambia. Our results indicate drier and warmer conditions under Green Sahara conditions relative to the Dry Sahara periods. In particular, an increase in the length of droughts and higher temperature extremes have been simulated over the Zambian region in the Green Sahara experiment. Our results suggest that during the Dry Sahara periods, Zambia may have offered better environmental conditions for hominin populations than the Central African Plateau (CAP). In contrast, the Green Sahara periods offered opposite conditions, potentially encouraging hominins to disperse through the large river valleys into the CAP and northward into the Sahel and Sahara.

Keywords: Green Sahara, Zambia, climate extremes, hominid dispersal.

1.1   Introduction

Recent archaeological and paleontological evidence suggests a complex, pan-African origin for our species, *Homo sapiens*, in which Sub-Saharan Africa (SSA) played a key role (Hublin *et al.*, 2017 ; Klein & Richard Klein, 2019 ; Scerri, 2017; Stringer & Galway-Witham, 2017 ; Wilkins, 2021). Past climate variability in SSA, and specifically in South Tropical Africa, is believed to have influenced human population dynamics and evolution at the scale of the African continent (Blome *et al.*, 2012 ; John E. Kutzbach *et al.*, 2020). Today, climate variability affects the socioeconomic development in this region, including food security and decent housing conditions. Therefore, it is imperative to identify the factors that control the development of a hydrological network and the climatic cycles that influence it.

SSA is dominated by a central plateau of more than 1 million km^2, bordered to the northeast by the Western Rift of Tanzania and Malawi, to the southeast by the Luangwa and Upper-Zambezi Rifts, and the northwest by the Upemba Rift (Daly *et al.*, 2020). The plateau is drained by the Zambezi, the third-largest hydrological network on the African continent. This drainage system, which passes through Zambia before flowing into the Indian Ocean, is considered by archaeologists to be an important biogeographic corridor, potentially influencing the pattern of hominin occupation of the region during the Stone Age with potential repercussions on human evolution in Africa (Larry Barham, 2000 ; Burrough *et al.*, 2019 ; Colton *et al.*, 2021).

Precipitation rates during the monsoon season exhibit large oscillations over a range of timescales, from interannual to interdecadal and longer periods (Mason & Jury, 1997 ; Richard *et al.*, 2001 ; Fauchereau *et al.*, 2003). On interannual timescales, for example, heavy rainfall can affect the region with daily precipitation locally exceeding 200 mm

(Manhique *et al*., 2015). Prolonged droughts, such as the one in 1991-1992, can also occur, causing crop failure and decreased livestock production (Vogel & Drummond, 1993). On longer timescales, the African continent has undergone pronounced climate shifts since the late Miocene (~11.6 to 5.3 Ma years ago). The most notable of these events is the so-called African Humid Periods (AHPs), during which the West and East African Monsoon intensifies and the Intertropical Convergence Zone (ITCZ) is displaced northward, transforming the hyper-arid Sahara Desert into a mesic environment (Gasse *et al*., 1990 ; deMenocal & Tierney, 2012) and affecting the climate worldwide (Pausata *et al*., 2017a, b ; Sun *et al*. 2019 ; Piao *et al*., 2020 ; Pausata *et* al., 2021 ; Dandoy *et al*., 2021). Evidence for AHPs exists in diverse paleoclimatic records (Hoelzmann *et al*., 1998 ; deMenocal *et al*., 2000 ; Hély *et al*., 2014 ; Tierney *et al*., 2017) and the last AHP occurred between about 11000 and 5000 years ago, when the present-day Sahara Desert was vegetated with a mixture of forests and grasslands, and several large lakes were present (Yu & Harrison, 1996 ; Gasse, 2000 ; Castañeda *et al*., 2009).

AHPs are a direct response of the African monsoon to the precession cycle, a periodic variation in Earth's orbit around the sun (Berger, 1978). During AHPs, the Earth is closer to the sun during boreal summer and farther away during boreal winter than today, leading to warmer summers and colder winters in the Northern Hemisphere. The warmer summers in the Northern Hemisphere caused a northward extension of the Hadley circulation, which allowed the West African Monsoon (WAM) to penetrate further north (Kutzbach, 1981 ; Gaetani *et al*., 2017). This brings heavy precipitation to the Saharan region (Kutzbach & Liu, 1997 ; Tierney *et al*., 2017) and leads to the greening of the present Sahara Desert, with Sahel-like vegetation reaching as far north as 28-30°N (Hély *et al*., 2014). The waxing and waning of the WAM over the last eight million years (Larrasoaña *et al*., 2013) may have impacted human evolution and dispersal throughout Africa.

Previous studies suggest that pluvial corridors created in the Sahara region during the AHPs may have favored hominin dispersals, influencing human evolution (Szabo *et al*., 1995 ; Osborne *et al*., 2008 ; Castañeda *et al*., 2009 ; Drake *et al*., 2011 ; Smith, 2012 ; Hublin *et al*., 2017). Researchers have recently proposed that our human lineage evolved on a continental scale, as climatic cycles reconnected populations in the "cradle of humankind" in South Africa with populations elsewhere in Africa (Hublin *et al*., 2017). The exact dispersal routes are still a subject of debate, but AHPs are thought to have influenced their development (Agustí & Lordkipanidze, 2011 ; Abbate & Sagri, 2012 ; Reynolds, 2015 ; Timmermann & Friedrich, 2016). A similar dynamic is suggested for the south tropical zone of Africa, where the Central Plateau and the Kalahari Desert cycled from arid to relatively humid conditions, potentially limiting the distribution of hominin populations and enhancing the importance of major watercourses such as the Zambezi as potential "refugia" (Burrough *et al*., 2019).

To our knowledge, no study has hitherto investigated the impact of AHPs in Tropical Africa south of the equator. The geographic position of this region, which lies between southern Africa and the East African Rift, where hominins likely first evolved, and northern Africa, where the most ancient proof of the existence of *Homo sapiens* is known (Hublin *et al.*, 2017 ; Richter *et al.*, 2017), means that this region is critical for our understanding of the dynamics of human biocultural evolution in Africa.

In this study, we use a regional climate model to simulate archetypal Green and Desert Sahara periods under high and low boreal summer insolation and investigate the changes in climate variability and extremes in southern Tropical Africa with a focus on its central region, Zambia. The goal of this research is to shed light on the changes in precipitation and temperature variability and extremes in the region associated with the waxing and waning of the WAM. These results may then help constrain the impact of climate change on the course of human evolution and dispersal.

This paper is structured as follows: the data and methodology are described in Section 2, the results are presented in Section 3, and the discussion and conclusions are presented in Section 4.

1.2 Data and methods

1.2.1 Model description

The Regional Climate Model (RCM) employed in this study is the developmental version of the Canadian Regional Climate Model 5th generation (CRCM5) based on the Global Environment Multiscale 4 (GEM4) model (Girard *et al*., 2014 ; McTaggart-Cowan *et al*., 2019) developed by the Recherche en Prévision Numérique (RPN) and the Canadian Meteorological Centre (CMC). The subgrid-scale physical parameterizations include the Kain & Fritsch (1990) deep-convection and Kuo-transient (Kuo, 1965) shallow-convection schemes, as well as the large-scale condensation scheme (Sundqvist *et al*., 1989) the correlated-K scheme for solar and terrestrial radiations (Li & Barker, 2005), a sub-grid-scale mountain gravity-wave drag (McFarlane & A., 1987) and low-level orographic blocking (Zadra *et al*., 2003), a turbulent kinetic energy closure in the planetary boundary layer and vertical diffusion (Benoit *et al.*, 1989 ; Delage & Girard, 1992 ; Delage, 1997), and a weak ∇^6 lateral diffusion. The land-surface scheme, however, is changed from Interaction Sol-Biosphère-Atmosphère (ISBA) used at CMC for the Canadian LAnd Surface Scheme (CLASS) (Verseghy, 2000, 2008) to its most recent version, CLASS 3.6. For these simulations, 16 soil layers are used, reaching a depth of 10 m. The standard CLASS distributions of sand and clay fields, as well as the bare soil albedo values, are replaced with data from the ECOCLIMAP database (Masson *et al*., 2003). Finally, the interactive thermodynamic 1-D lake module (FLake model) is also used (Martynov *et al*. 2010, 2012).

1.2.2 Study area and its climate

The model domain covers the entire SSA (10°N–35°S; 15°W – 55°E) with a primary focus on Zambia (Figure 1.1). Three areas within Zambia were chosen for more detailed analysis: Northeastern Zambia (10.82°S; 33.07°E), Central Luangwa River Valley (13.19°S; 31.71°E), and Zambia's capital city, Lusaka (15.42°S; 28.28°E). Lusaka is located at the southern end of the Central African Plateau (CAP). We chose the Central Luangwa River Valley because it forms part of the Zambezi watershed, a major hydrological system that drains central Africa. Recent studies have highlighted archeological evidence of hominin occupations in the area from the middle Pleistocene onwards as well as evidence of important climatic fluctuations (Barham *et al*., 2011 ; Colton *et al*., 2021 ; Burke *et al*., 2021).

Central southern Africa is a region that lies in the tropics and experiences a monsoon climate with high annual and interannual rainfall variability (Mason & Jury, 1997; Richard *et al*., 2001 ; Fauchereau *et al.*, 2003). At these timescales, three different contributions of surface airstreams influence the rainfall pattern in central southern Africa (Nicholson, 2019). Firstly, southeastern trade winds originate over the Indian Ocean to the east and the south of Africa as well as northeasterly monsoonal flow from the Indian subcontinent. All of them are thermally stable with subsiding dry air (Nicholson, 2019). Warm and humid easterly trade winds meet at the ITCZ. When the high insolation season in boreal summer occurs, the ITCZ moves northward toward the area of low pressure over the Sahara Desert and the dry southeast trades control the central southern African climate. On the contrary, in January, when the ITCZ is further south, heavy rain is expected in central southern Africa as the convergence zone moved southward (Nicholson, 2019). The third airstream is a westerly flow that comes from the South Atlantic Ocean and converges with the two latter easterly currents (Nicholson, 2019). The airstream flows across the Congo basin and cools to saturation due to the

high elevation of eastern Africa, bringing heavy rain (Nicholson, 2019). The Southeastern Africa monsoon is associated with a period of heavy rainfall lasting from November to April with the precipitation peaking from December to February.

1.2.3 Experimental design

We use model output from global simulations carried out by Pausata *et al*. (2016) and Gaetani *et al*. (2017) with an Earth System Model (EC-Earth version 3.1) at a horizontal resolution of $1.125° \times 1.125°$ and 62 vertical levels for the atmosphere to drive regional simulations at the lateral and lower boundaries at a horizontal resolution of $0.11°$ (~12 km).

We carry out the following three simulations (Table 1.1): 1) the pre-industrial (PI) climate in which PI greenhouse gases (GHGs) and current vegetation cover are prescribed to represent the low insolation – dry Sahara case (LI_{DS}). The other two idealized simulations are performed under middle Holocene (MH) solar orbital forcing 6000 years ago. 2) Concerning the LI_{DS} simulation, we only change in the first MH sensitivity simulation the GHGs and the orbital forcing which are set as MH, following the Paleoclimate Intercomparison Project phase 3 (PMIP3) protocol (Taylor e*t al*., 2009). The boundary conditions are the same as those for the LI_{DS} simulation. This experiment represents the high insolation – dry Sahara (HI_{DS}), i.e., a transition state at the end of the AHPs. 3) In the second MH experiment, the lower and lateral boundary conditions are changed as well, using output from a global model experiment in which the Saharan surface (11°–33°N, 15°W–35°E) was changed from desert to shrubs, and PI dust concentrations are reduced by up to 80% (for more details see Gaetani e*t al.* (2017) and Pausata *et al.* (2016). This experiment represents the high insolation – green Sahara (HI_{GS}). Each simulation is 30 years long. The LI_{DS} is the reference simulation for desert Sahara conditions and low boreal summer insolation, while the HI_{GS} is the reference simulation for the green Sahara state and high boreal summer insolation.

Daily maximum and minimum temperatures and precipitation are used to analyze the changes in climatology and climate extremes.

1.2.4 Climate extreme indices

Daily temperature and precipitation data are used to calculate extreme climate indices. Here, we use temperature and precipitation climate indices defined by the Expert Team on Climate Change Detection and Indices (ETCCDI) (Zhang *et al.,* 2011). They defined a set of extreme climate indices based on temperature and precipitation. In this study, we examine the changes in selected indices for the 30 years of each simulation, as we display their spatial distribution over the entire SSA domain. These indices fall into four categories, i.e., absolute indices, threshold indices, duration indices, and percentile indices. From the 27 available indices in the ETCCDI, we selected the six most commonly used (Table 1.2). In particular, we chose the annual maximum daily maximum temperature or the hottest day of the year (TXx), the annual minimum daily minimum temperature or the coldest night of the year (TNn), and the number of tropical nights per year (TRn), that is, the number of nights in which the minimum temperature does not fall below 20°C. We also considered the number of consecutive dry days (CDD) that constitutes the maximum number of consecutive days in a given year with precipitation less than 1 mm, that is, the longest dry spell of the year. The annual maximum precipitation amount fallen over five consecutive days (RX5day), which is used to identify prolonged heavy rainfall events, and the number of wet days per year in which the daily precipitation exceeds 1 mm (R1mm). The statistical significance of the changes was estimated based on the Student two-tailed *t test* (Yuen & Dixon, 1973) and the non-parametric Wilcoxon signed-rank test (Wilcoxon, 1945) at the 5% significance level.

1.3   Results

In this section, we first present the annual and seasonal climatological changes in the temperature and precipitation distribution in the SSA domain during the high boreal summer insolation periods relative to the reference period of low boreal summer insolation (Subsection 1.3.1). We then investigate how climatological changes during high insolation periods are reflected in terms of changes in climate extremes over Zambia relative to low insolation periods (Subsection 1.3.2). Finally, we discuss changes in the seasonal cycle of temperature and precipitation at specific sites in Zambia (Subsection 1.3.3).

1.3.1   Changes in the annual and seasonal climatology of temperature

Zambia lies in the tropics, and its climate is characterized by two seasons: a dry season from May to October with a core ranging from June to August and a wet season from November to April, peaking from December to January. The annual temperature for the LI_{DS} simulation ranges from 16 to 22°C in Zambia (Figure 1.2a). More specifically, mean temperatures of 17.4°C, 17.5°C, and 21.4°C were simulated in our three sub-regions (northeastern Zambia, Lusaka, and Central Luangwa River Valley, respectively). The model has a cold bias in the region of approximately 2-2.5°C. For instance, in Lusaka, the present-day observed annual mean temperature is 19.9°C for the 1961-1990 period (National Oceanic and Atmospheric Administration – NOAA[1]), whereas the simulated pre-industrial temperature is approximately 17.5°C. In the dry season, from May to October, the simulated seasonal mean temperature is slightly

---

[1] https://www.ncei.noaa.gov/access/monitoring/products/

cooler in Lusaka (16.1°C), followed by NE Zambia (16.5°C) and Central Luangwa River Valley (20.4°C) (Figure 1.2d). The observed 1961-1990 dry season temperature is 18.3°C in Lusaka (NOAA[1]), which is 2.2°C warmer than the simulated temperature for the region. As for the LI_{DS} humid season (November–April), simulated temperatures in the region range mainly between 18°C and 24°C (Figure 1.2 g). In the Central Luangwa River Valley, it is considerably warmer than the two other locations because of its lower elevation as it reaches a seasonal mean of 22.3°C compared to 18.4°C in NE Zambia and 18.8°C in Lusaka. The observed 1961-1990 humid season temperature is 2.7°C warmer than the simulated temperature in Lusaka with an average of 21.5°C (NOAA[1]).

The mean annual temperature in the insolation alone (HI_{DS}) experiment compared to LI_{DS} generally shows a slight significant cooling over Zambia, up to 0.5°C in the north-western area (Figure 1.2b). The only exception is represented by the region in the southeastern part, where the mean annual temperature is not significantly affected by changes in insolation alone (Figure 1.2b). During the dry season, the HI_{DS} exhibits small significant cold anomalies over southwest (SW) Zambia near Lusaka, up to approximately 0.25°C, whereas temperatures in the northeast (NE) near the Central Luangwa River Valley region do not show any significant change (Figure 1.2e). During the wet season, a slight but significant cooling is simulated in the HI_{DS} experiment compared to the LI_{DS} simulation over most of Zambia, peaking in the northern area with anomalies of up to 0.5°C (Figure 1.2h). The significant cooling also characterizes the region of the three selected areas with negative anomalies of approximately 0.25°C. The greening of the Sahara and dust reduction (Figure 1.2c) show statistically significant warm anomalies between 0.25°C and 0.50°C for the entire Zambian subdomain relative to the LI_{DS} experiment. Over the central and eastern parts of the subdomain, the dry season temperature is higher than in the LI_{DS} experiment, by up to 0.6°C in the NE part of Zambia (Figure 1.2f), whereas the western part does not show

a significant change compared to the LI$_{DS}$ experiment. Finally, in the wet season, significant positive anomalies occur in the region with up to 0.5°C (Figure 1.2i) in the HI$_{GS}$ simulation relative to the LI$_{DS}$ experiment.

In summary, slight cooling is simulated in all seasons for the HI$_{DS}$ experiment relative to the LI$_{DS}$, being more pronounced in the wet season. Whereas, significant warming during the entire year is shown in the HI$_{GS}$ compared to the LI$_{DS}$.

1.3.2 Changes in the annual and seasonal climatology of precipitation

The annual mean rainfall in Zambia ranges between 2 and 6 mm/day in the LI$_{DS}$ simulation (Figure 1.3a), with higher precipitation amounts in the northern section of the country. For example, the model simulates an annual rainfall of 3.1 mm/day for Lusaka, about 3.7 mm/day for River Valley, and up to 4.2 mm/day for NE Zambia. The observed 1961-1990 precipitation in Lusaka is lower than that in the LI$_{DS}$ simulation, amounting to approximately 2.4 mm/day (NOAA[1]). During the dry season, from May to October, precipitation is very low with a simulated rainfall mean below 0.5 mm/day across the region (Figure 1.3d), which compares well to the 1961-1990 Lusaka's observed precipitation reaching 0.13 mm/day (NOAA[1]). During the wet season, i.e., from November to April (Figure 1.4g), the main part of the annual precipitation occurs in Lusaka with an average of 5.9 mm/day of rainfall throughout that season, Central Luangwa River Valley averaged 6.9 mm/day and NE Zambia received 7.8 mm/day. The 1961-1990 observed precipitation for Lusaka is 4.7 mm/day (NOAA[1]), which is 1.2 mm/day lower than the simulated precipitation.

Changes in the climatological mean precipitation over the study region do not show a clear signal in the HI$_{DS}$ experiment relative to the LI$_{DS}$. In particular, the orbital forcing experiment alone (HI$_{DS}$) does not lead to statistically significant changes in annual

precipitation for most of Zambia (Figure 1.3b). As the dry months are characterized by scarce rainfall, no large change in precipitation is expected, with no significant changes in precipitation in the HI_{DS} experiment relative to the LI_{DS} during the dry season (Figure 1.3e). During the wet season, an increase in precipitation in most locations of up to 0.6 mm/day is simulated in the HI_{DS} experiment relative to the LI_{DS} (Figure 1.3h) in NE Zambia; however, the precipitation changes are generally statistically non-significant in all the locations.

The HI_{GS} experiment relative to the LI_{DS} shows a slight decrease in annual rainfall over the three study locations, being most pronounced in Lusaka (0.2 mm/day) (Figure 1.3c). Moreover, a significant reduction in precipitation (up to 0.25 mm/day) is simulated in the HI_{GS} experiment across central southern Africa during the dry season (Figure 1.3f). In the wet season, the Lusaka region sees significant reductions in precipitation of 0.25 mm/day in the HI_{GS} experiment relative to the LI_{DS} (Figure 1.3i).

In summary, significant negative changes in precipitation are simulated in the HI_{GS} experiment over the whole Zambia subdomain in the dry season, and over the CAP (0.25 mm/day) in the wet season. The overall annual precipitation slightly decreases in Lusaka (0.2 mm/day) in the HI_{GS} experiment relative to the LI_{DS}, although the changes are not significant. The HI_{DS} experiment does not show any significant annual and seasonal change relative to LI_{DS}.

1.3.3   Changes in climate extremes: indices of temperature

Changes in solar insolation alone (HI_{DS}) lead to a temperature increase for the hottest day of the year (TXx) of up to 1.2°C relative to the LI_{DS} experiment, throughout Zambia, especially in the southern part (Figure 1.4a). In contrast, the lowest temperature of the year (TNn) is lower in the HI_{DS} experiment (Figure 1.4c). Relative to the LI_{DS}, it

exhibits a decrease of up to 0.5°C in TNn in the NE part of Zambia, and a more notable decrease of 0.7°C is simulated in the Lusaka and Central Luangwa River Valley region, and a decrease of up to 1.5°C in the southwestern part of the country, including the CAP (1°C). An increase in the number of tropical nights (TRn) of about five nights is simulated for the HI$_{DS}$ experiment for the River Valley relative to the LI$_{DS}$ simulation. On the other hand, no statistically significant TRn change was detected for NE Zambia and Lusaka (Figure 1.4e).

When considering the changes in Saharan vegetation and dust concentration (HI$_{GS}$), the pattern in TXx changes is similar to the HI$_{DS}$ pattern, however, the positive anomalies are amplified with values up to 3°C in the SE part of the country, including Central Luangwa River Valley and Lusaka locations. Over the CAP, the temperature anomalies are slightly less pronounced (~2°C) (Figure 1.4b). The pattern in TNn changes for the HI$_{GS}$ experiment is comparable to that of the HI$_{DS}$, although the negative anomalies are amplified: 1.5°C over the CAP and nearly 1°C in the Central Luangwa River Valley (Figure 1.4d). The River Valley has seen a significant increase of 14 TRn in the HI$_{GS}$ experiment relative to the LI$_{DS}$, while no statistically significant TRn change was simulated for the two other locations (Figure 1.4f).

Overall, our results show that Sahara greening plays an important role in affecting temperature extremes, leading to more extreme temperatures in southern tropical Africa for both the low and high values relative to HI$_{DS}$ and LI$_{DS}$ simulations with major differences between the Central Luangwa River Valley and the CAP.

1.3.4   Changes in climate extremes: indices of precipitation

The orbital forcing alone (HI$_{DS}$) causes an increase in the drought duration over the entire Zambia subdomain (Figure 1.5a) as shown by the changes in consecutive dry days annual means (CDD). This increase is generally not significant, except for the SE area. The CAP region, including Lusaka, presents the higher CDD anomalies with an increase of 23 days (22%), followed by the NE part of Zambia with 22 days (34%), and finally the Central Luangwa River Valley region with an increase in CCD of 12 days (16%). The 5-day maximum precipitation amount (RX5day) also intensified as rainfall increased, ranging from 7 mm in Lusaka (7%) and the Central Luangwa River Valley (5%) to nearly 13 mm in NE Zambia (8%) (Figure 1.5c). No significant change in the total number of rainy days (R1mm) is simulated under insolation forcing alone (Figure 1.5e).

Saharan vegetation and reduction in dust concentrations (HI$_{GS}$) increase the CDD over all of Zambia, amplifying the anomalies observed in the HI$_{DS}$ experiment, particularly in the southern and western parts of the country (Figure 1.5b). An increase of 27 CDD is simulated in the Central Luangwa River Valley, more than doubling compared to the HI$_{DS}$, and the lowest increase is now found in NE Zambia with 25 CDD relative to the LI$_{DS}$. The longest duration of dry spells is simulated in Lusaka, with an increase of over a month (39 days) in CDD relative to the LI$_{DS}$ experiment. The RX5d index presents similar, albeit weaker, results for the HI$_{GS}$ simulation as for the HI$_{DS}$ (Figure 1.5d), with all the changes being not statistically significant. In the HI$_{GS}$ experiment, the number of rainy days (R1mm) is significantly decreased by up to 12 days in Lusaka, followed by NE Zambia and Central Luangwa River Valley with a decrease of 11 and 9 days respectively relative to the LI$_{DS}$ (Figure 1.5f).

In summary, the combined effect of increased boreal summer insolation and Sahara greening causes drying in the study region during all seasons. Drought duration is

enhanced in the HI_{GS}, as shown by the number of consecutive dry days, especially over the CAP (39 days), followed by the Central Luangwa River Valley (27 days) compared to the LI_{DS} experiment. A significant decrease in rainy days is shown by HI_{GS} relative to the LI_{DS} during the wet season over the whole region where the selected areas lie.

1.3.5 Regional changes in seasonal cycles of mean temperature and precipitation

In this section, we present the temperature and precipitation seasonal cycles of all three experiments; for simplicity, we only show NE Zambia; however, the results are similar for all of Zambia. The temperature peaks in the pre-monsoonal season with the warmest month in October, while the coldest season is from May to July with the coldest month in June. The rainfall seasonality is characterized by a dry season with no or little rainfall from May to October and a rainy season from November to April.

The seasonal temperature cycle shows a temperature increase at the end of the dry season, from September to November, in the HI_{DS} simulation relative to the LI_{DS} (Figure 1.6a). The temperature increase is nearly 0.5°C in September and November, with a significant peak of approximately 1.5°C in October. Throughout the remainder of the year, no significant temperature changes were simulated in the HI_{DS} experiment.

Saharan vegetation change and dust reduction during a Green Sahara state (HI_{GS}) present similar result. However, the temperature change is amplified from September to November, with higher significant values of nearly 1.5°C and 2°C in September and November, respectively, and a peak in October of about 2.5°C relative to the LI_{DS}. As in the HI_{DS}, the HI_{GS} shows no statistically significant temperature change throughout the rest of the year relative to the LI_{DS}.

In the HI simulations, the climatological seasonal precipitation cycle exhibits an increase during the core of the humid season in December and January, relative to the LI$_{DS}$ (Figure 1.6b). Rainfall increases up to 2.5 and 3 mm/day for HI$_{DS}$ and HI$_{GS}$ in December and January, respectively. A small reduction of nearly 0.5 mm/day is simulated for both HI simulations relative to the LI$_{DS}$ at the start of the humid season in October and November and at the start of the dry season in March and April. Throughout the rest of the year, from May to September, no statistically significant precipitation change is simulated.

In conclusion, our simulations show a shift forward in the rainfall associated with the summer monsoon and enhanced aridity in the dry season. The decrease in precipitation in the dry season in the HI simulations relative to the LI experiment is associated with an increase in the divergence aloft that intensifies in the HI$_{GS}$ relative to HI$_{DS}$ (Figure 1.7). Such an increase in the divergence aloft enhances arid conditions during the dry season over Zambia (Figures 1.3e and f, 1.5a and b). The average monthly temperature increases in the pre-monsoonal season (August through November) in the HI$_{GS}$ relative to the LI$_{DS}$. The fall and early winter temperatures (February to June) are instead below average. Such anomalous behavior is identical in the HI$_{DS}$ and HI$_{GS}$ experiments, as it is mostly driven by the changes in solar insolation with an increase in late winter and spring insolation (August to November) and a decrease during summer and fall (December to May). However, the temperature anomalies in the HI$_{GS}$ are larger than in the HI$_{DS}$ in austral winter due to warmer advection as the temperature in central and eastern equatorial Africa are remarkably higher (compare panels e and f in Figure 1.2). The more pronounced anomalies simulated in the HI$_{GS}$ relative to the HI$_{DS}$ experiments highlight the far-reaching role of vegetation.

1.4   Discussion and conclusions

In this study, we show that vegetation changes over the Sahara and the associated reduction in airborne dust concentrations during periods of high boreal summer insolation (HI$_{GS}$) remarkably impact temperature and rainfall in SSA and Zambia, in particular. During the HI$_{DS}$, the changes in annual and seasonal temperature in Zambia are small, being only slightly warmer than in the LI$_{DS}$. From September to November, temperature and precipitation extremes change significantly under HI$_{GS}$ conditions relative to the low insolation and dry Sahara (LI$_{DS}$) case. In particular, the hottest day (TXx) and the coldest night of the year (TNx) become more extreme with an increase of up to 3°C and a decrease of up to 1.5°C, respectively. The number of rainy days (R1mm) decreases by approximately 10 days in Lusaka relative to the LI$_{DS}$ experiment, which has a total of 102 rainy days per year. This means that, in the HI$_{GS}$ experiment, there is a 10% reduction in the number of rainy days per year. Droughts also become more extended under HI$_{GS}$ conditions relative to the LI$_{DS}$ conditions, with an increase in CDDs of over a month in the southern part of Zambia. Overall, the model simulates hotter AHP conditions in southern tropical Africa. The results also show a major difference in rainfall changes and the length of droughts between the CAP and the Central Luangwa River Valley. These results highlight the potentially crucial role played by the Zambezi drainage and the Luangwa River Valley as key water resources for seasonal hominin mobility, especially during the dry season.

The simulated changes in temperature and precipitation over Zambia are largely a result of changes in solar insolation and the modification in the atmospheric dynamics induced by the strengthening of the West African Monsoon. In general, the anomaly pattern seen in the HI$_{GS}$ experiment relative to the LI$_{DS}$ is very similar to the HI$_{DS}$, but it is more intense, highlighting the central role of the West African Monsoon in altering

atmospheric circulation over Africa and hence affecting southern tropical Africa. In Zambia, the impact of these changes is also influenced by local topography, with distinctly drier and more drought-prone conditions in the Central Plateau relative to the Zambezi drainage during the HI_{GS} relative to the LI_{DS}. The insolation changes during the mid-Holocene (i.e., higher insolation from June to November and lower from December to May) are responsible for the higher temperature extremes (Figures 1.4a and b) as well as a higher number of tropical nights (Figures 1.4e and f). Temperature extremes in Zambia are recorded in the pre-monsoonal dry season, i.e., from September to November, which coincides with the increase in insolation in the region. The decrease in insolation during the boreal summer and fall (January to May) is causing lower monthly mean temperatures up to the beginning of winter (Figure 1.6a), explaining the drop in low-temperature extremes (Figures 1.4c and d). Therefore, changes in temperature extremes, despite no changes or slight cooling in the annual mean, are essentially due to increased insolation between July and November and decreased insolation between December and May.

Although we use the middle Holocene and pre-industrial boundary conditions and orbital forcing, our simulations can be seen as archetypal of other high and low boreal summer insolation forcing. However, MH orbital forcing was far from being extreme: for example, summer insolation was much stronger during the Eemian (128,000 – 122,000 years ago) or even during the early Holocene (11,000 – 8,000 years ago; Otto-Bliesner *et al.*, 2016).

The extreme conditions seen in our HI_{GS} scenario may have altered patterns of hominin mobility, thus affecting the course of hominin evolution in Africa, and were likely even more extreme during other HI periods, when insolation changes were even larger than those simulated in our experiments. According to our simulations, the CAP experienced less rainfall during the dry season, from May to October, under AHP

conditions with an increase in the number of consecutive dry days and more arid conditions. On a regional scale, the savanna landscapes of the CAP would consequently have changed, becoming less favorable for human habitation, especially during the extended dry season. As the CAP became less hospitable, the resources offered by large river drainages such as the Zambezi and its tributaries, such as the Luangwa River, would have been critical to hominin survival, guiding their seasonal mobility (Barham, 2000 ; Burrough *et al.*, 2019). The fluctuation between more aridity during the AHPs and less aridity during the dry Sahara in the Luangwa Valley also has implications for the inferred depositional history of the region and thus, the regional archaeological record (Colton *et al.*, 2021 ; Burke *et al.*, 2023). More arid conditions in the CAP, which would have seasonally constrained human mobility, occurred at a time when hydrological systems in the Sahel and the Sahara were activated, opening "green corridors" that would have facilitated genetic and cultural exchange on a continental scale, once again highlighting the importance of Central African river systems. Given the recurrence of the AHPs, our results would imply a cyclicity in the pattern and the timing of population migration across northern and central Africa with serious implications for the pattern of hominin evolution, as has recently been suggested (Hublin *et al.*, 2017).

In conclusion, the results of this study show that AHPs affect Southern Tropical Africa making it a more arid environment overall - possibly constraining hominin mobility at a time when movement across the Sahara Desert would have been possible. This could have enhanced the role of large river systems such as the Luangwa River, which would have acted as refugia and biogeographic corridors (Barham, 2000 ; Barham *et al.*, 2011). Perhaps not coincidentally, hominin occupations in the Luangwa Valley occurred under more arid conditions (Colton *et al.*, 2021). Continuing archaeological research in the Luangwa Basin may help resolve whether climatic fluctuations drove patterns of human occupation and movement in the area during prehistory (Burke *et al.*, 2023).

Acknowledgments

Data availability

Data for this paper can be requested to F.S.R.P. (pausata.francesco@uqam.ca)

TABLEAUX

Table 1.1   Boundary conditions prescribed for pre-industrial (PI) reference control and mid-Holocene (MH) climates.

	GHGs	**Orbital forcing years B.P.**	**Saharan vegetation**	**Saharan dust**
LI$_{DS}$	PI	0	Desert	PI
HI$_{DS}$	MH	6000	Desert	PI
HI$_{GS}$	MH	6000	Shrubs	Reduced

Table 1.2   List of six climate indices used in this study out of the 27 from ETCCDI and their definitions.

Label	**Definition of index**	**Unit**
TXx	Annual maximum value of daily maximum temperature	°C
TNn	Annual minimum value of daily minimum temperature	°C
TRn	Annual number of nights with temperature $\geq 20°C$	Nights
CDD	Annual maximum number of consecutive days with Rain Rate (RR) < 1 mm	Days
RX5d	Annual maximum consecutive 5-day precipitation amount	Mm
R1mm	Annual number of days with RR > 1 mm	Days

FIGURES

Entire domain and Zambia subdomain
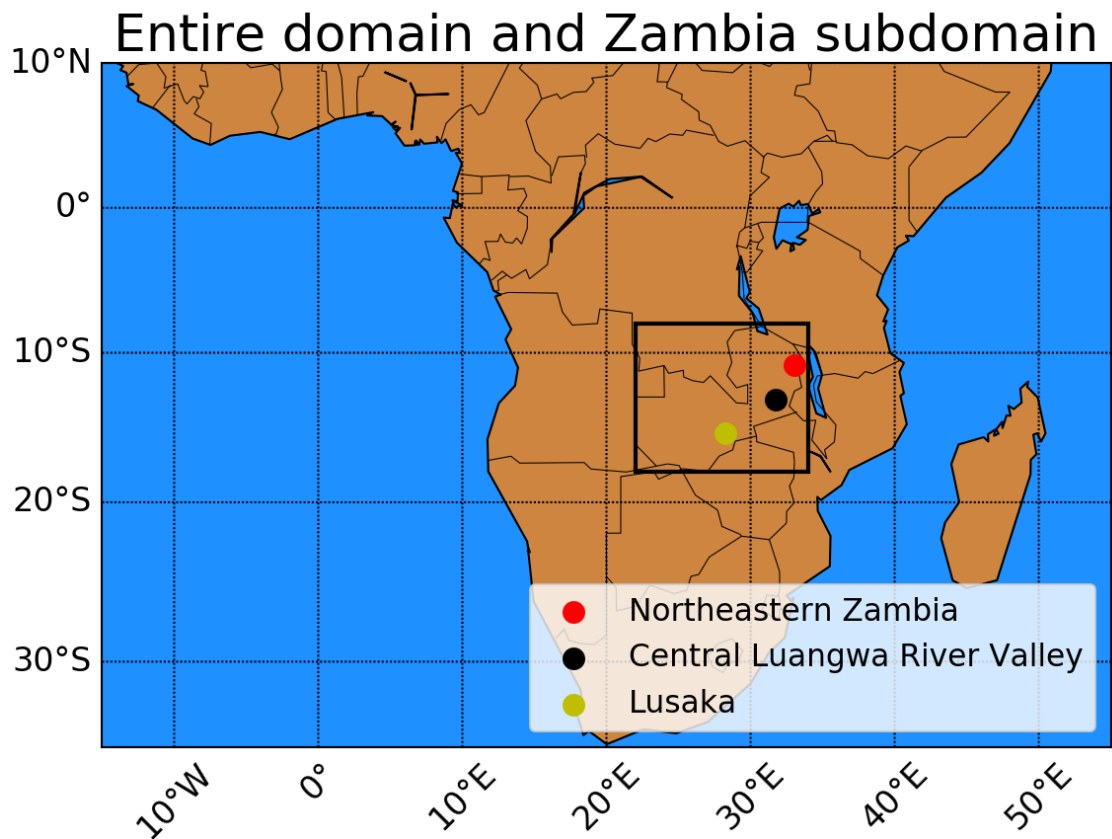
Figure 1.1 Study area: entire regional climate model domain and the Zambia subdomain (black rectangle) and the three subregions more extensively discussed (colored dots).
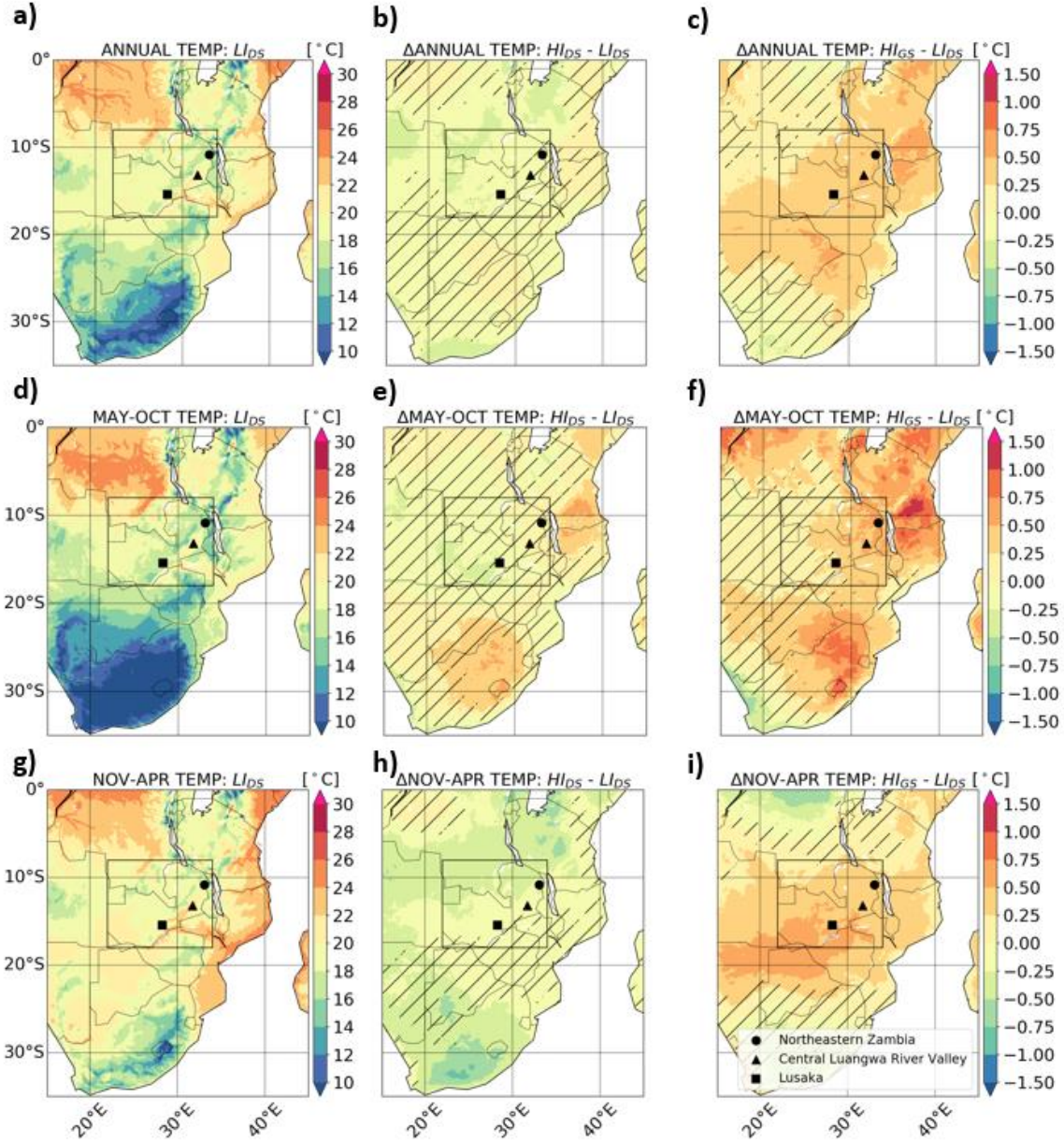
Figure 1.2 Mean temperature for Low Insolation Dry Sahara (LI$_{DS}$) experiment (a-c) and anomalies for the High Insolation – Dry Sahara (HI$_{DS}$) (d-f) and the High Insolation – Green Sahara (HI$_{GS}$) (g-i) simulations for the annual (a, d, g), May-October (b, e, h,) and November-April (c, f, i) climatology relative to LI$_{DS}$. Non-statistically significant anomalies at the 5% significance level are hatched.
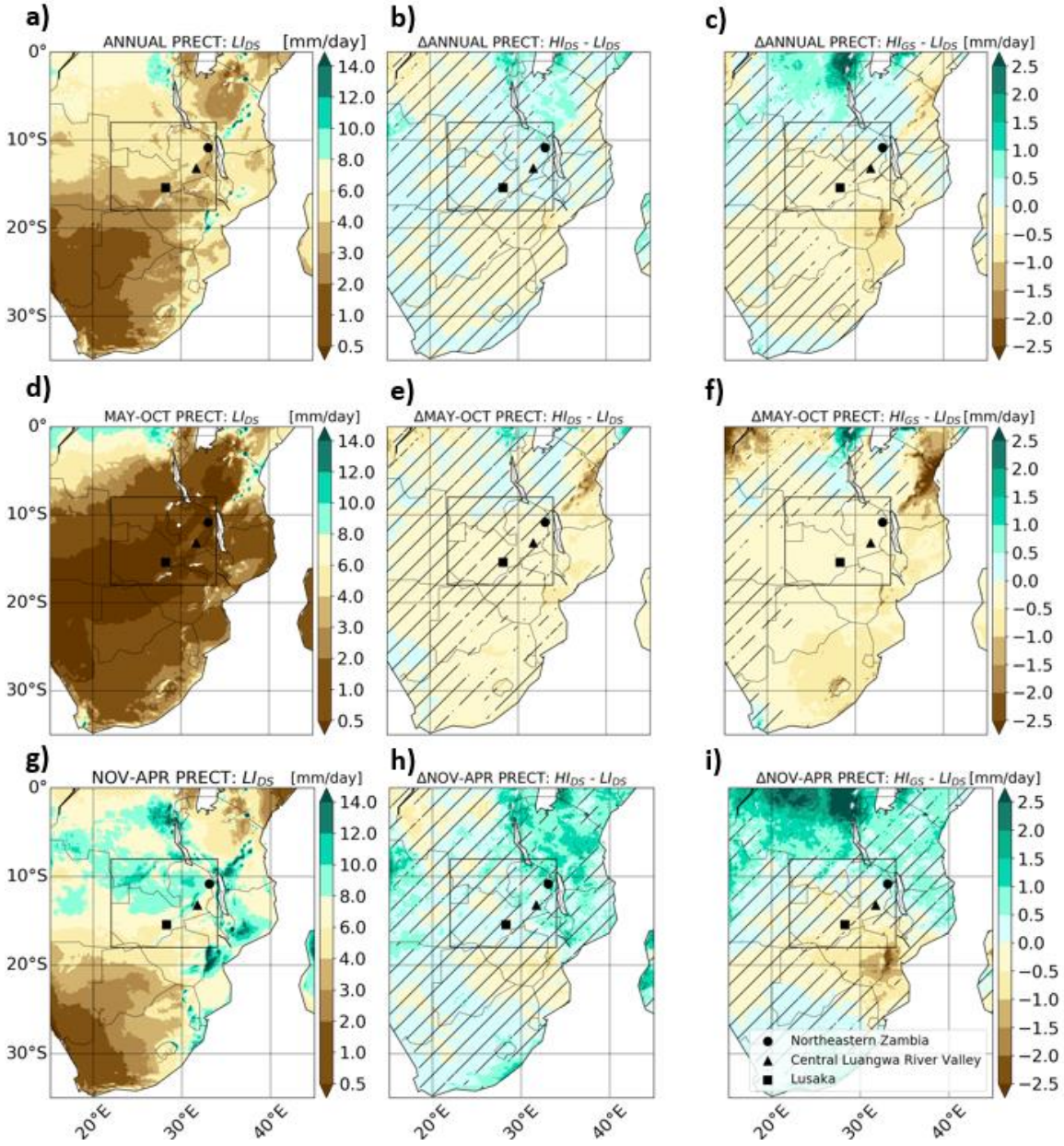
Figure 1.3 Mean precipitation for Low Insolation - Dry Sahara (LI$_{DS}$) experiment (a-c) and anomalies in the High Insolation - Dry Sahara (HI$_{DS}$) (d-f) and in the High Insolation Green Sahara (HI$_{GS}$) (g-i) simulations for the annual (a, d, g), May-October (b, e, h) and November-April (c, f, i) climatology relative to LI$_{DS}$. Non-statistically significant anomalies at the 5% significance level are hatched.
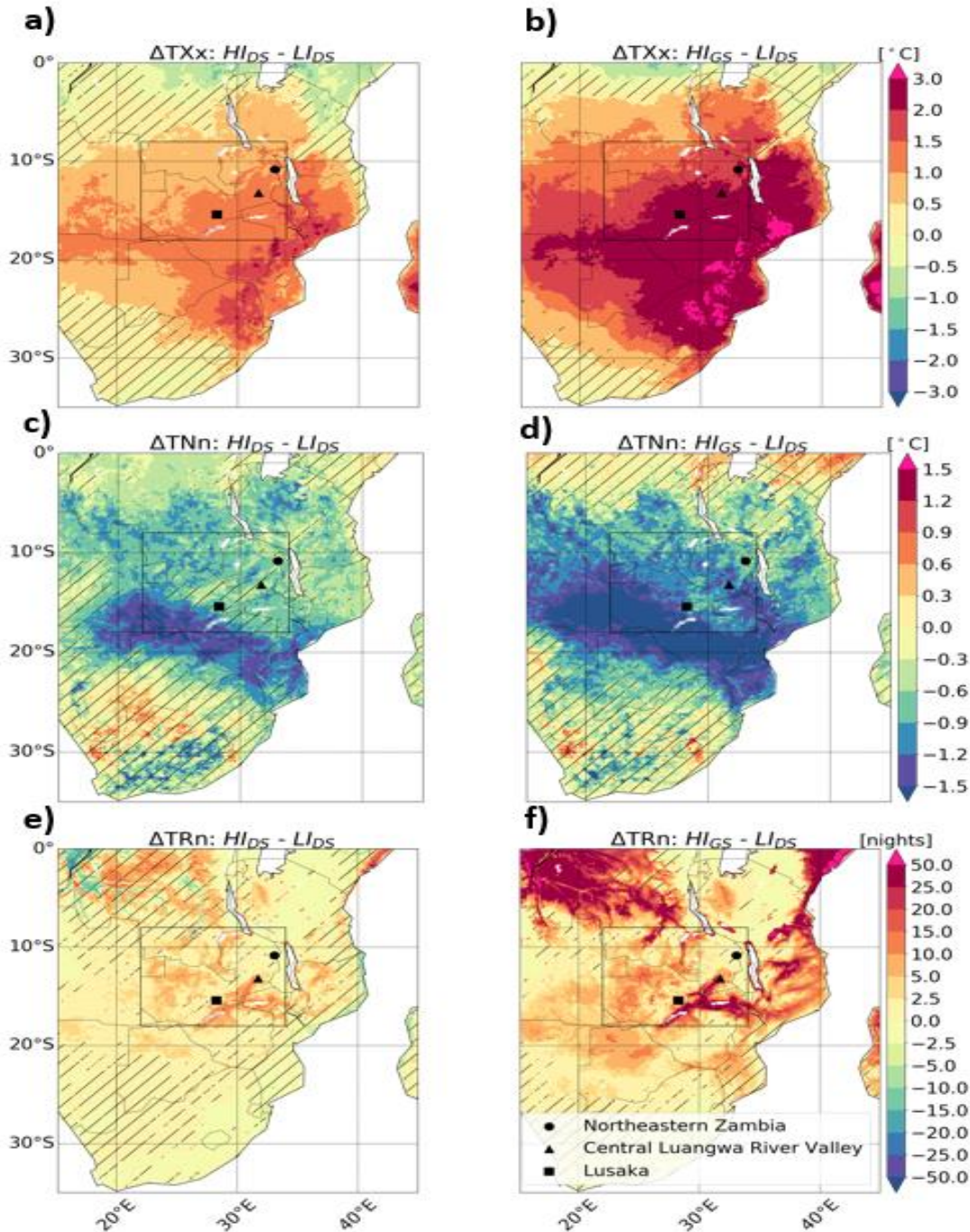
Figure 1.4 Changes in the temperature of the annual hottest day (TXx, (a) and (b)), coldest night (TNn, (c) and (d)), and in the number of tropical nights (TRn (e) and (f)) for the HI$_{DS}$ and HI$_{GS}$ experiments relative to the LI$_{DS}$ simulation. Non-statistically significant anomalies at the 5% significance level are hatched.
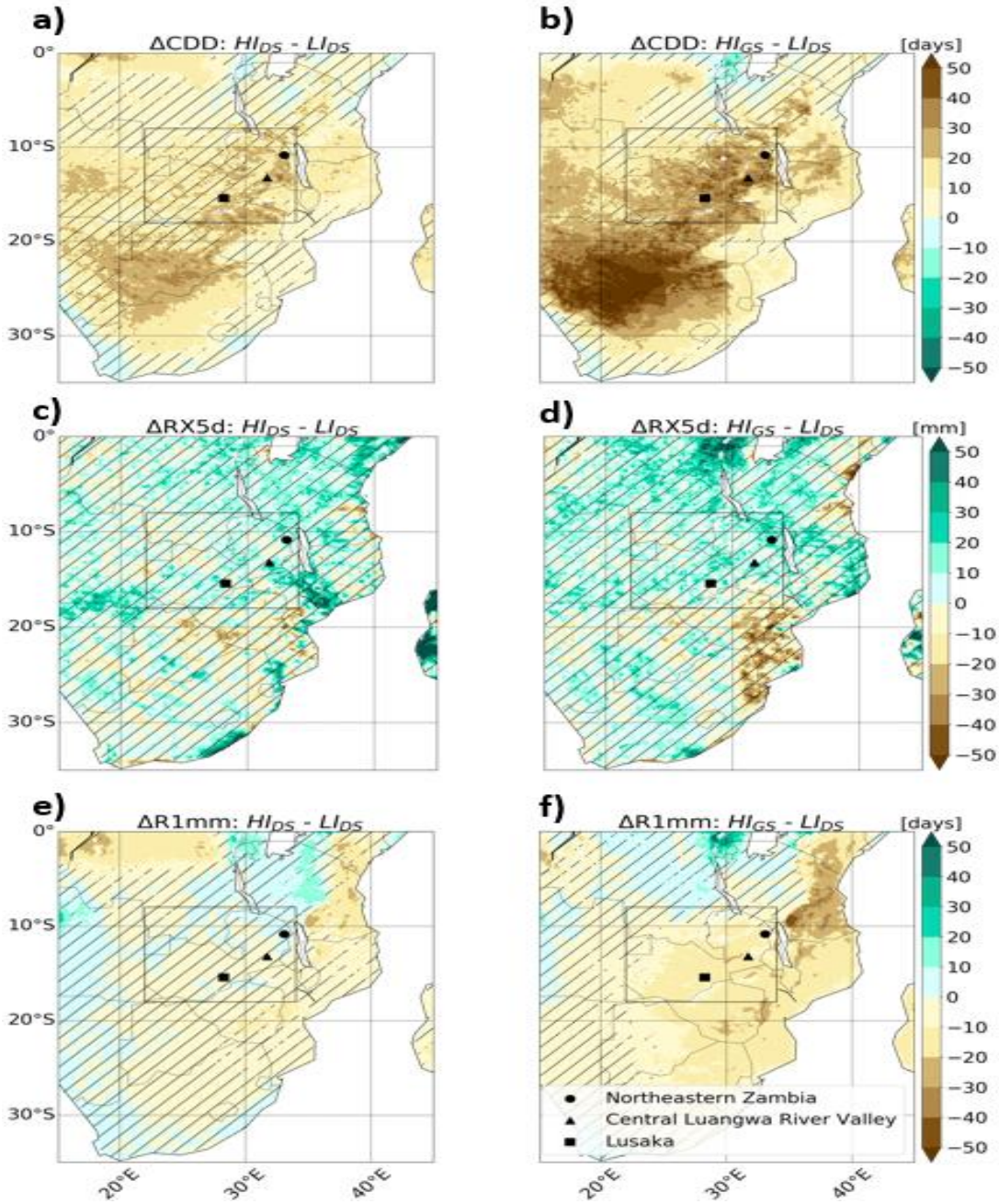
Figure 1.5 Changes in the annual consecutive dry days (CDD, (a) and (b)), 5-day maximum precipitation (RX5day, (c) and (d)), and in the number of rainy days (R1mm (e) and (f)) for the HI_{DS} and HI_{GS} experiments relative to the LI_{DS} simulation. Non-statistically significant anomalies at the 5% significance level are hatched.
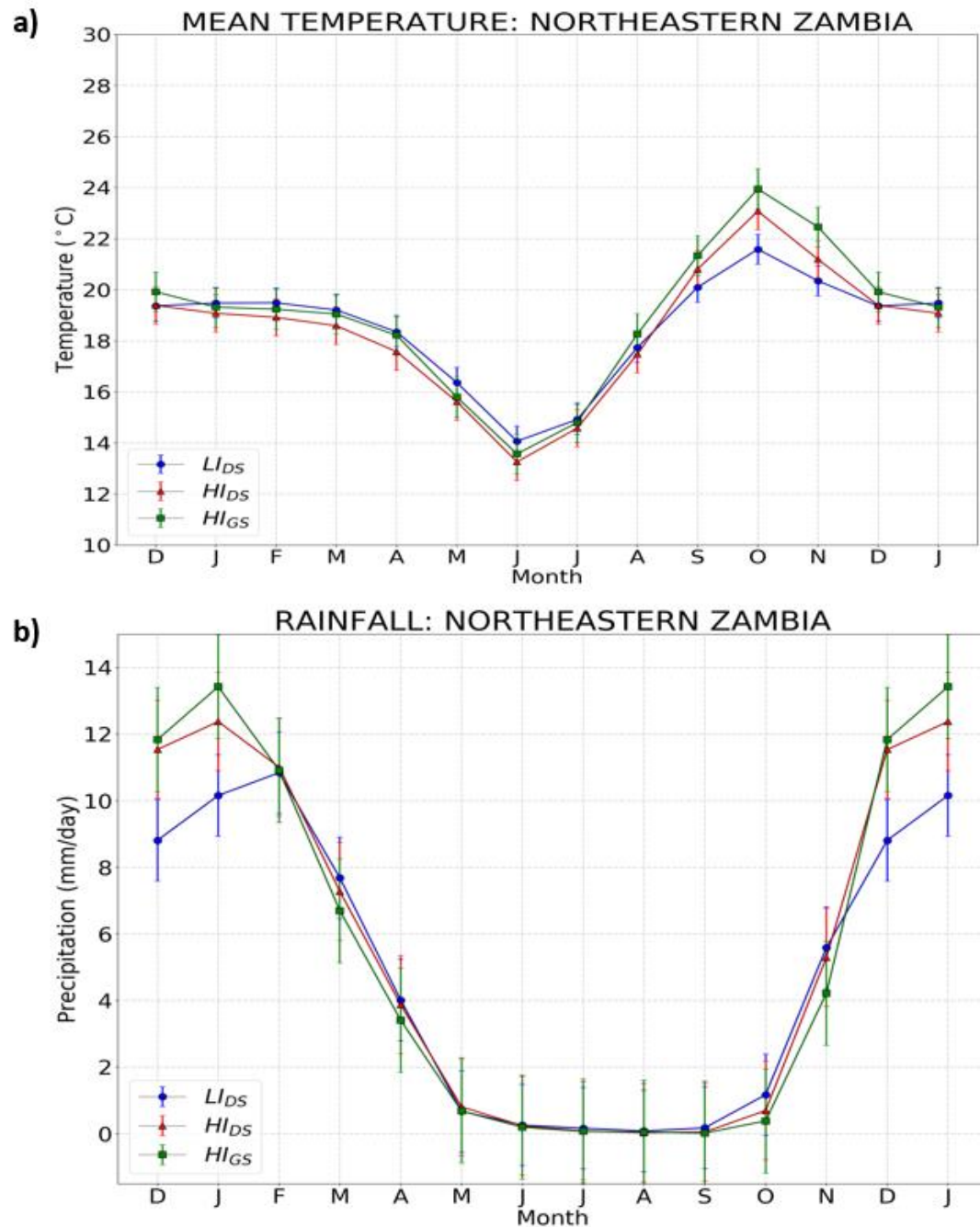
Figure 1.6 a) Temperature and b) precipitation climatological seasonal cycle in northeastern Zambia (10.82°S; 33.07°E) for LI_{DS} (blue), HI_{DS} (red), and HI_{GS} (green) simulations. Error bars indicate the standard error of the mean.
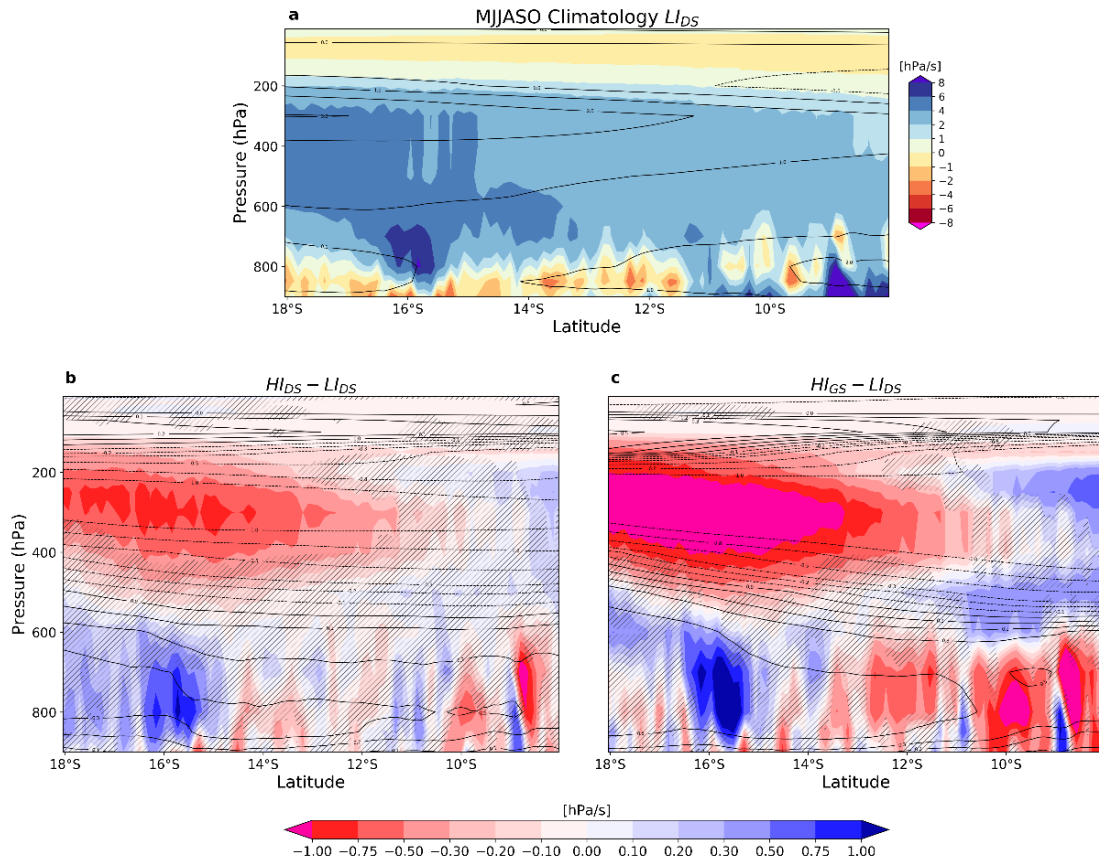
Figure 1.7 Meridional and vertical circulation. a) Climatological meridional circulation (contours, m/s) and vertical motion (shaded) averaged between 22°E and 35°E for the period May-October (MJJASO) and their changes for b) HI_{DS} and c) HI_{GS} relative to pre-industrial (L_{IDS}). Positive (blue) values of vertical motion indicate downward motion while positive values of meridional circulation indicate northward direction. Hatched areas cover the areas where the changes are not statistically significant at 5% of the significance level.

SUPPLEMENTARY MATERIAL

SUPPLEMENTARY FIGURES

Standardized Temperature Index (STI)

In this study, we used the Standardized Temperature Index (STI). It represents the probability of the occurrence of a temperature value when compared with temperature values over a longer period. This can be useful in identifying unusually hot and cold periods.

$$STI = \frac{T - T*}{\sigma T}$$

Where

T = Temperature

T = Mean temperature

σ_T = Standard deviation of temperature

STI values are categorized into different groups.

« Extremely hot»   when   STI >= 2.00

« Very hot»   "   STI >= 1.50 and < 2.00

« Moderately hot»   "   STI >= 1.00 and < 1.50

« Near normal»   "   STI <   1.00 and > -1.00

« Moderately cold»   "   STI <= -1.00 and > -1.50

« Very cold»   "   STI <= -1.50 and > -2.00

« Extremely cold»   "   STI <= -2.00

Standardized Precipitation Index (SPI)

We also use the Standardized Precipitation Index (SPI), which was originally described by McKee *et al.* (1993). As for STI, SPI represents the probability of occurrence of a precipitation value when compared with precipitation values over a longer period. It is useful for identifying droughts and floods.

It is based only on precipitation and can be used on different timescales such as 3-, 6-, 9-, 12-, 24-, and 48-month time scales.

A **12-month** SPI is a comparison of the precipitation for 12 consecutive months with the same 12 consecutive months during all previous years of available data. The SPI at these time scales shows *long-term precipitation patterns*. Because these time scales are the cumulative result of shorter periods that may be above or below normal, the longer SPIs tend toward zero unless a specific trend occurs.

$$\text{SPI} = \frac{(P - P*)}{\sigma p}$$

Where

P = Precipitation

P = Mean precipitation

σ_p = Standard deviation of precipitation

Similar to the STI, SPI values are categorized into different groups.

« Extremely wet»	when	SPI >= 2.00
« Very wet»	"	SPI >= 1.50 and < 2.00
« Moderately wet»	"	SPI >= 1.00 and < 1.50
« Near normal»	"	SPI < 1.00 and > -1.00
« Moderately dry»	"	SPI <= -1.00 and > -1.50
« Very dry»	"	SPI <= -1.50 and > -2.00
« Extremely dry»	"	SPI <= -2.00

In this study, we developed an algorithm that averages the maximum temperature (TMAX) and minimum temperature (TMIN) for 30 years of data in a square that roughly covers Zambia (8°-18°S; 22°-32°E) to reproduce density charts for both temperature variables and the three simulations (LI_{DS}, HI_{DS}, HI_{GS}).
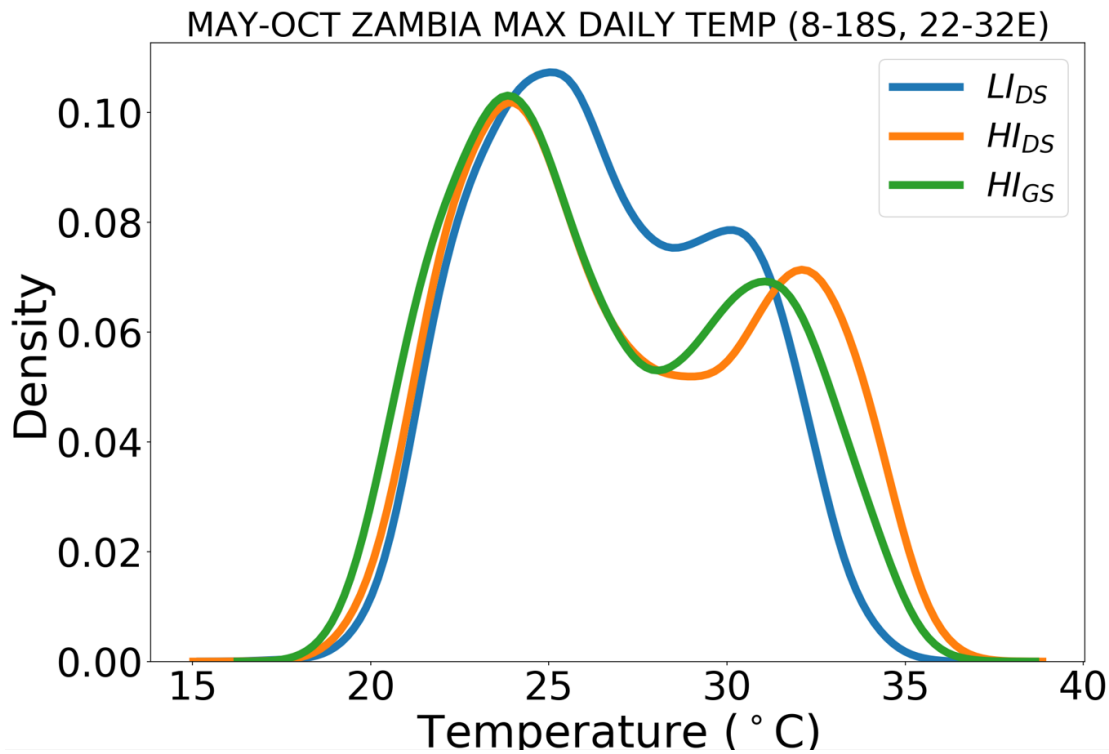
Figure S1   Density for the May to October (May-Oct) averaged maximum daily temperature in the 22-32°E; 8-18°S Zambia region for LI_{DS} (blue), HI_{DS} (orange), and HI_{GS} (green) simulations.

During the dry season, we can observe two means in Figure S1 for all three experiments. Under LI conditions, the graph shows that the means are closer to each other, meaning maximum daily temperatures are less extreme than under HI conditions. Also, the right side of the graph shows that higher daily maximum temperatures occur more frequently under HI conditions.
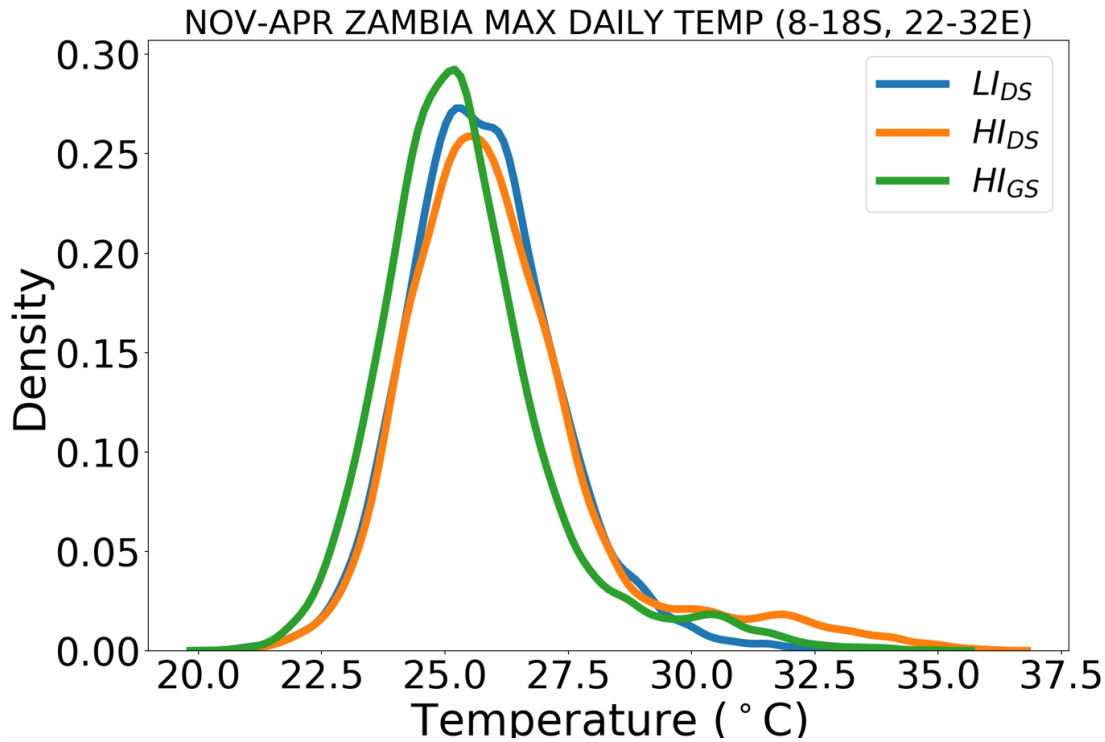
Figure S2   Density for November to April (Nov-Apr) averaged maximum daily temperature in the 22-32°E; 8-18°S Zambia region for LI_{DS} (blue), HI_{DS} (orange), HI_{GS} (green) simulations.

For the HI_{DS} experiment, we can see the mean daily maximum temperature shift to the right, meaning warmer temperatures during the day. We also notice that both sides show more extreme temperatures under HI conditions.
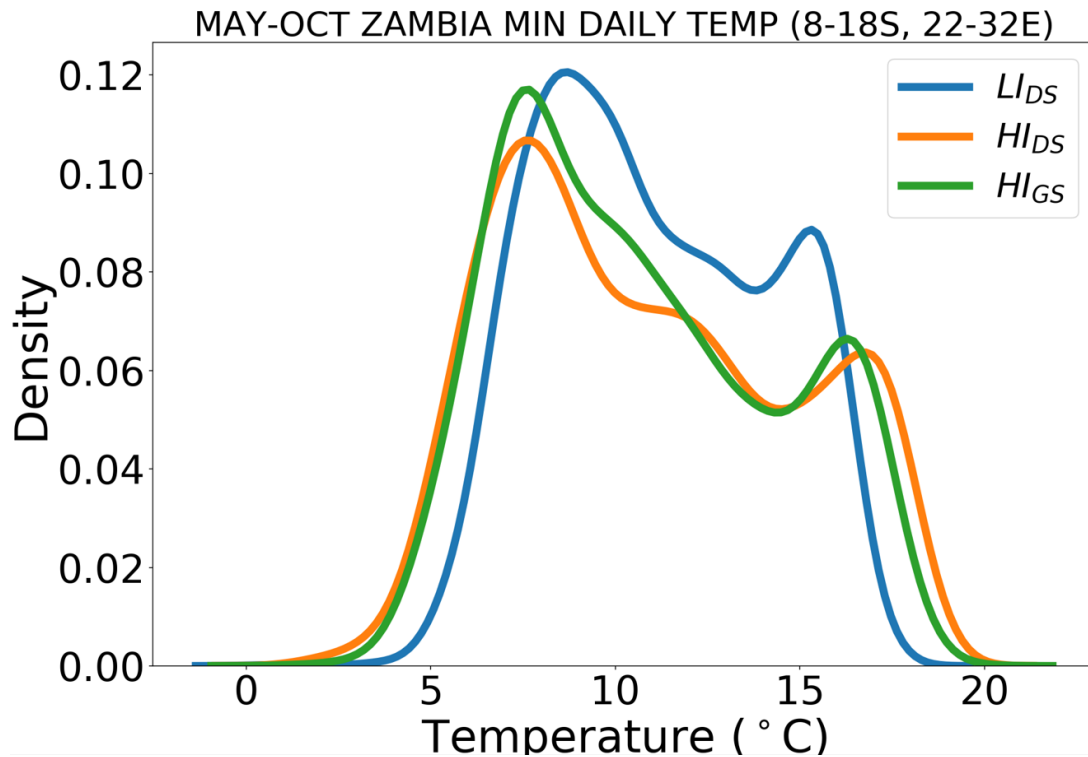
Figure S3   Density for May to October (May–Oct) averaged minimum daily temperature in the 22-32°E; 8-18°S Zambia region for LI_{DS} (blue), HI_{DS} (orange), HI_{GS} (green) simulations.

Here, the graph shows that the minimum daily temperature has mainly two means. Under HI conditions, the left mean shift to the left compared to LI conditions, meaning more extreme cold temperatures. Furthermore, the right mean shift to the right under HI conditions compared to LI conditions, meaning more extreme hot temperatures for the mimimum daily temperature throughout the dry season.
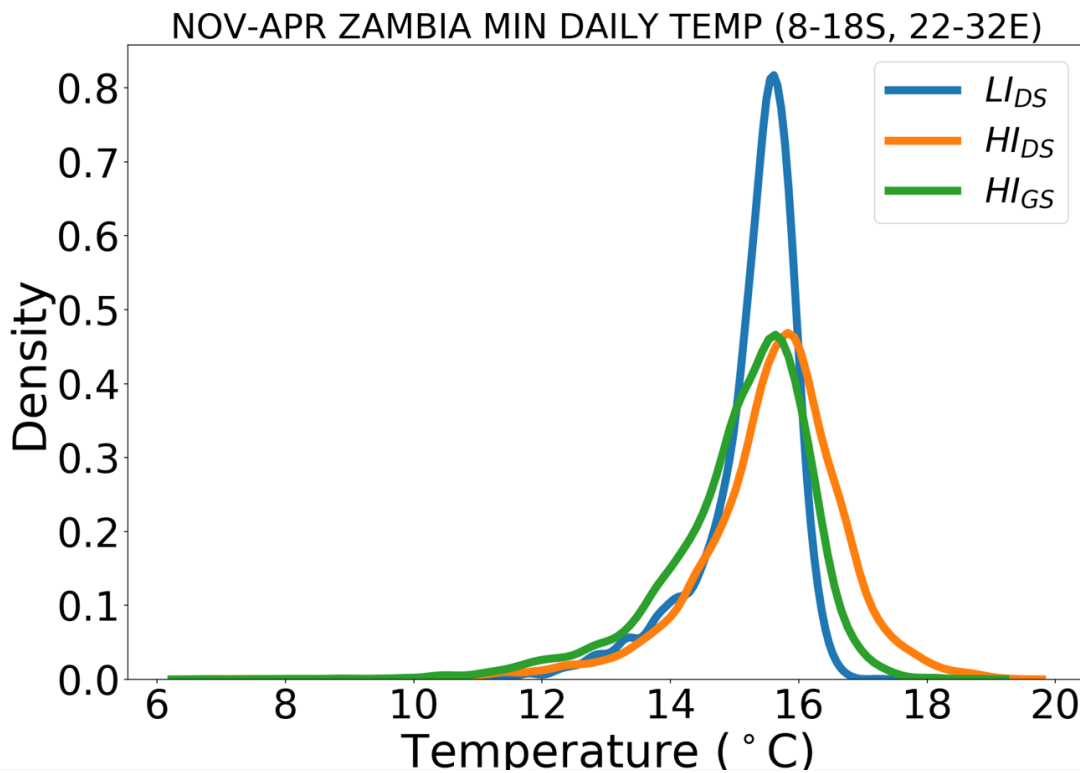
Figure S4 Density for the November to April (Nov-Apr) averaged minimum daily temperature in the 22-32°E; 8-18°S Zambia domain for LI_{DS} (blue), HI_{DS} (orange), and HI_{GS} (green) simulations.

The graph for the minimum daily temperature throughout the wet season mainly shows that under HI conditions, the standard deviation increases compared to LI conditions. It shows that the mean is nearly the same, however, we can notice more extremes in both cold and hot minimum daily temperatures for the HI conditions compared to the LI conditions.

$LI_{DS}+HI_{GS}$: 2-30yr STI-12 for 3 regions in Africa CS
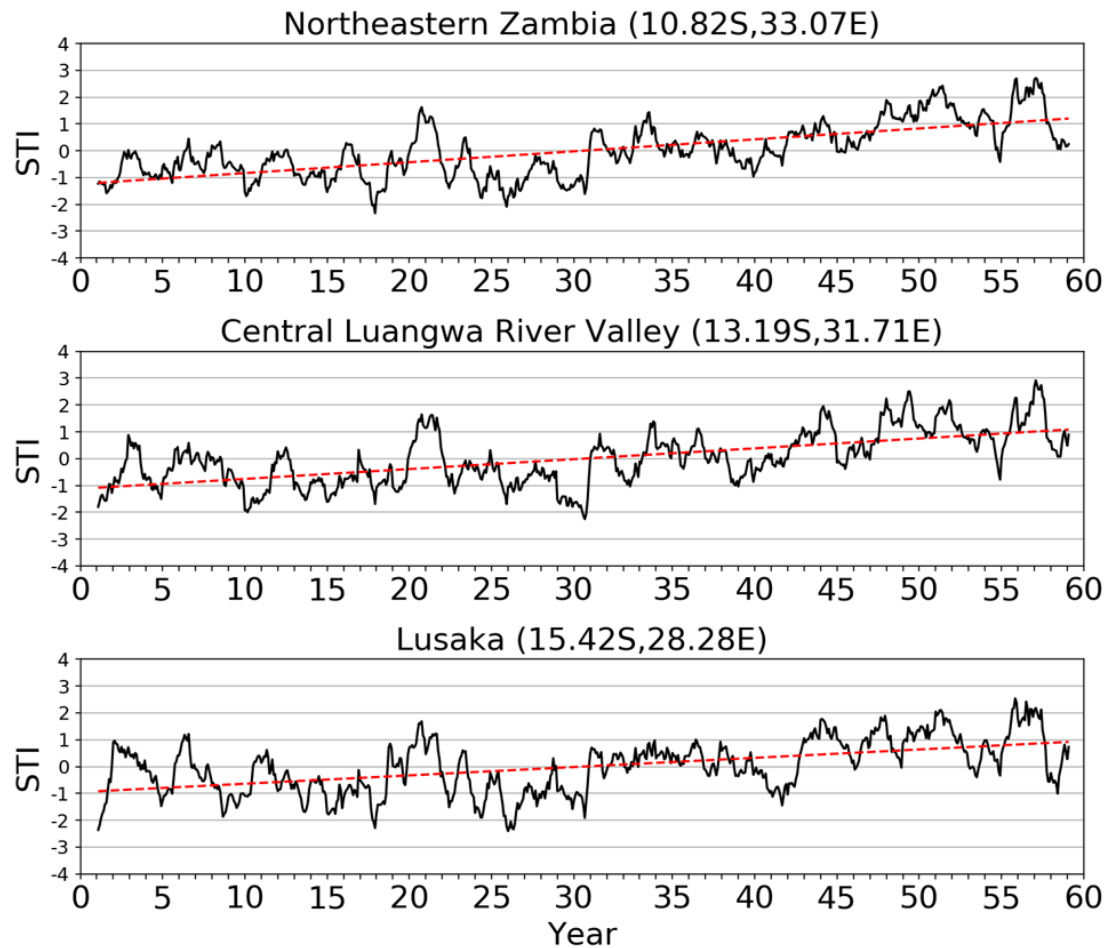
Figure S5 LI_{DS} + HI_{GS} 12-month Standardized Temperature Index (STI-12) (black line) for 2-30 years in Northeastern Zambia, Central Luangwa River Valley, and Lusaka locations. The dashed red line follows a linear trend.
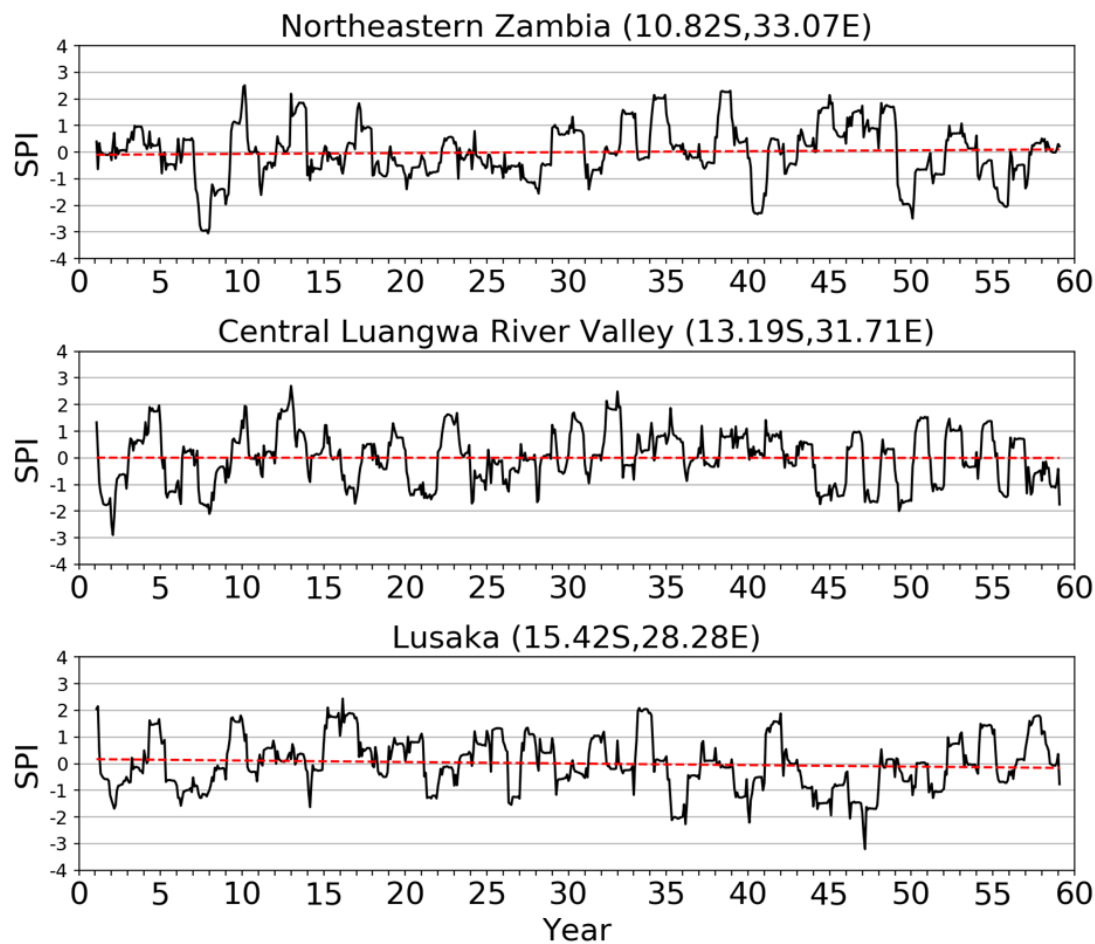
Figure S6 LI$_{DS}$ + HI$_{GS}$ 12-month Standardized Precipitation Index (SPI-12) (black line) for 2-30 years in Northeastern Zambia, Central Luangwa River Valley, and Lusaka locations. The dashed red line follows a linear trend.

CONCLUSION

Afin de compléter cette étude, nous avons réalisé trois expériences en utilisant le modèle régional canadien du climat (MRCC6) à haute résolution dans le but d'étudier le rôle de la haute insolation par précession, de la couverture végétale dans le Sahara et de la diminution de poussière sur le mouvement des hominidés en Afrique subsaharienne lors des périodes chaudes du Sahara vert durant l'Holocène moyen, il y a environ 6000 ans. Grâce aux observations paléoclimatiques, nous savons que cette période chaude transformait l'Afrique du Nord en environnement plus favorable pour les hominidés, puisque le Sahara était dorénavant recouvert de végétation du fait que l'insolation estivale causée par le changement en précession a renforcé la MOA.

Deux expériences avec un climat de l'Holocène moyen ont été comparées par rapport à l'ère préindustrielle, la première étant celle qui correspond au forçage orbital durant l'Holocène moyen (étés plus chauds dans l'HN) qui renforce les moussons et la deuxième qui englobe la réduction de poussière et la couverture végétale dans le Sahara pendant l'Holocène moyen. Cela a permis de constater que les changements dans la végétation et la réduction de poussière lors des périodes de haute insolation en été boréal (HI_{GS}) ont un impact sur la température et la précipitation en ASS et particulièrement en Zambie.

Nos simulations démontrent un décalage vers l'avant de la précipitation au cours de la mousson estivale et une aridité accrue lors de la saison sèche. La réduction de précipitation durant la saison sèche dans les simulations à haute insolation par rapport à celle de basse insolation est associée à une divergence en altitude qui s'intensifie lors

de périodes du Sahara vert et une haute insolation en été dans l'HN par rapport à une période sèche (Figure 1.7). Une telle augmentation de la divergence en altitude renforce les conditions arides pendant la saison sèche en Zambie (Figures 1.3e, f et 1.5a, b). La température mensuelle moyenne augmente lors de la saison précédant la mousson (août à novembre) dans l'expérience HI_{GS} par rapport à l'expérience LI_{DS}. La température automnale et au commencement de l'hiver (février à juin) est plutôt sous la moyenne. De telles anomalies sont identiques dans les expériences HI_{DS} et HI_{GS}, puisqu'elles sont principalement conduites par les changements en insolation, c'est-à-dire une augmentation tard en hiver et au printemps (d'août à novembre) et une réduction durant l'été et l'automne (décembre à mai). Toutefois, les anomalies de températures dans l'expérience HI_{GS} sont plus importantes que dans l'expérience HI_{DS} lors de l'hiver austral, car les advections en température dans le centre/est équatorial de l'Afrique sont plus chaudes (Figure 1.2 e et f). Les anomalies en température simulées sont davantage marquées dans la HI_{GS} comparé aux expériences HI_{DS} et soulignent le rôle majeur de la végétation. Tandis que les changements annuels de température dans la simulation HI_{DS} sont faibles, étant légèrement supérieurs comparés à la simulation LI_{DS}, et ce, surtout de septembre à novembre; les changements en température et précipitation sont significatifs sous la simulation HI_{GS} par rapport à la simulation LI_{DS}. Les extrêmes climatiques sont d'autant plus grands lors des périodes de haute insolation, comme on peut le voir dans les diagrammes de densité de températures maximales et minimales journalières en Zambie (Figures S1 à S4). En effet, lors de la saison sèche (Figures S1 et S3), les températures simulées minimales et maximales journalières en Zambie s'éloignent de la moyenne des deux côtés par une distribution des températures plus étalée (plus grand écart-type). Nous avons ainsi des températures minimales plus froides et des températures maximales plus chaudes, ce qui pourrait avoir modifié l'habitat et l'environnement des hominidés tels que la faune et la flore, rendant la disponibilité de la nourriture plus difficile, et de ce fait même forcer les hominidés à aller ailleurs. Pour les trois régions d'étude, l'index STI-12 suit une courbe linéaire de

-1 (modérément froid) à 1 (modérément chaud) pour une période de haute insolation avec végétation dans la région sahélienne et une réduction de poussière (HI$_{GS}$) comparée à une période de basse insolation (LI$_{DS}$) (Figure S5). Également, on peut constater ces extrêmes climatiques via les indices TXx et TNx qui sont plus extrêmes sous les conditions HI$_{GS}$, avec une augmentation jusqu'à 3°C et une réduction jusqu'à 1,5°C. Le nombre de jours pluvieux (R1mm) diminue de près de 10 jours à Lusaka, et le nombre simulé de jours pluvieux pour la simulation LI$_{DS}$ dans la région équivaut à 102, ce qui correspond à une diminution de près de 10 % pour le nombre de jours pluvieux par année dans la capitale. Les sécheresses sont également relativement prolongées sous les conditions HI$_{GS}$ par rapport à LI$_{DS}$, avec une augmentation de l'indice CDD de plus d'un mois dans le sud du pays. Globalement, nous avons vu des températures plus chaudes lors des périodes humides africaines dans la zone tropicale sud de l'Afrique. Les résultats ont démontré notamment un contraste majeur entre le CAP et la Central Luangwa River Valley pour ce qui est des changements de précipitation et la durée des sécheresses, renforçant l'importance des cours d'eau majeurs comme le fleuve Zambèze et la rivière Luangwa en tant que ressources clés pour la mobilité saisonnière des hominines, particulièrement lors de la saison sèche.

À grande échelle, les changements simulés résultent des changements dynamiques dans l'atmosphère, induits par le renforcement de la mousson ouest-africaine, plutôt qu'un effet direct des changements dans le taux de poussière en Zambie, ceux-ci étant négligeables. Les anomalies modélisées vues dans la simulation HI$_{GS}$ par rapport à LI$_{DS}$ sont très similaires à HI$_{DS}$, quoique plus intenses, soulignant la force de la mousson ouest-africaine, qui peut altérer la circulation atmosphérique sur tout le continent africain et de ce fait même affecter la zone tropicale sud. En Zambie, nous pouvons constater l'impact de la topographie sur ces changements par des conditions plus arides produisant des contrastes dans les conditions pour le plateau central par rapport au drainage du Zambèze lors du HI$_{GS}$ relatif au LI$_{DS}$. Les changements en insolation

pendant l'Holocène moyen (c'est-à-dire plus d'insolation de juin à novembre et moins d'insolation de décembre à mai) sont responsables pour les températures extrêmes (Figures 4a et b) ainsi qu'à un plus grand nombre de nuits tropicales (Figures 4e et f). Les températures plus extrêmes en Zambie sont enregistrées juste avant la mousson lors de la saison sèche, de septembre à novembre, ce qui coïncide avec l'augmentation en insolation dans la région. La réduction en insolation durant l'été boréal et l'automne (de janvier à mai) provoque une baisse dans les températures moyennes mensuelles jusqu'au début de l'hiver (Figure 1.6a), expliquant la réduction en basses températures extrêmes (Figures 1.4c et d). Par conséquent, les changements en extrêmes de température, malgré aucun changement ou un faible refroidissement dans la moyenne annuelle, sont essentiellement dus à l'augmentation en insolation de juillet à novembre ainsi qu'à la réduction en insolation de décembre à mai.

Bien que nous utilisions les conditions aux limites et le forçage orbital de l'Holocène moyen et préindustriel, nos simulations peuvent être considérées comme un archétype des autres forçages de basse ou haute insolation boréale estivale. Toutefois, le forçage orbital lors de l'Holocène moyen était loin d'être extrême: par exemple, l'insolation estivale était beaucoup plus intense durant l'Éémien (il y a 128,000 – 122,000 ans) ou même lors du début de l'Holocène (il y a 11,000 – 8,000 ans).

Des conditions extrêmes dans le scénario HI$_{GS}$ pourraient avoir eu un impact sur l'évolution des hominines et sur leur répartition spatiale à l'échelle continentale et régionale. Ces conditions étaient possiblement d'autant plus extrêmes durant d'autres périodes de haute insolation, lorsque les changements en insolation étaient plus grands que ceux simulés par nos expériences. Toujours selon nos simulations, le plateau central africain a reçu moins de pluie durant la saison sèche, de mai à octobre, sous les conditions vécues lors de la période humide africaine, c'est-à-dire avec un nombre de jours secs consécutifs plus grands et ainsi, des conditions plus arides.

À l'échelle régionale, les savanes zambiennes, qui forment une partie du plateau central africain, pourraient avoir été moins favorables pour l'habitation humaine, notamment pendant la saison sèche dorénavant allongée. Ceci est vrai pour toutes les périodes humides africaines pendant le Plio-Pléistocène, car l'obliquité est le stimulateur des périodes humides africaines. En Zambie, alors que le CAP devenait moins hospitalier, les ressources offertes par le drainage du Zambèze et de la rivière Luangwa qui en fait partie auraient été critiques pour la survie humaine, guidant leurs mouvements saisonniers (Barham, 2020 ; Burrough *et coll.*, 2019). À un moment où les systèmes hydrologiques se sont développés dans le Sahara et le Sahel, ouvrant des « corridors verts » de mouvement et ainsi un échange génétique et culturel sur l'échelle continentale. Étant donné la cyclicité des périodes humides africaines comme évènements climatiques, qui concordent avec les dépositions sédimentaires par exemple, dans la vallée Luangwa (Colton *et coll.*, 2021 ; Burke *et coll.*, 2023), cela implique une cyclicité dans le patron des occupations humaines et dans la chronologie des migrations de population à l'échelle de l'Afrique comme récemment suggéré (Hublin *et coll.*, 2017).

En conclusion, les résultats de cette étude démontrent que les périodes humides africaines affectent la zone tropicale sud de l'Afrique en la rendant plus aride globalement, contraignant potentiellement le mouvement des hominines à un moment que le déplacement à travers le Sahara aurait pu être possible. Cela aurait pu renforcer le rôle des grands cours d'eau comme la rivière Luangwa, qui aurait agi comme une zone refuge et de corridor biogéographique (Barham, 2000 ; Barham *et coll*., 2011). Poursuivre les recherches archéologiques dans les régions telles que le bassin de Luangwa pourrait confirmer si les fluctuations climatiques avaient été le moteur des occupations humaines et du mouvement dans la région pendant la préhistoire (Burke *et coll*., 2023).

BIBLIOGRAPHIE

Abbate, E., & Sagri, M. (2012). Early to Middle Pleistocene Homo dispersals from Africa to Eurasia: Geological, climatic and environmental constraints. Quaternary International, 267, 3–19. https://doi.org/10.1016/J.QUAINT.2011.02.043

Agustí, J., & Lordkipanidze, D. (2011). How "African" was the early human dispersal out of Africa? Quaternary Science Reviews, 30(11–12), 1338–1342. https://doi.org/10.1016/J.QUASCIREV.2010.04.012

Ahmadi, N., Asiedu, E. A., Baris, P., Boirard, H., Bricas, N., Cruz, J. F., ... & Zoungrana, B. (2013). Rainfed Food Crops in West and Central Africa. HAL.

Barham, Larry. (2000). The Middle Stone Age of Zambia, South Central Africa. Western academic & specialist Press. Retrieved from https://www.amazon.com.br/Middle-Stone-Zambia-Central-Africa/dp/095354186X

Barham, Lawrence, Phillips, W. M., Maher, B. A., Karloukovski, V., Duller, G. A. T., Jain, M., & Wintle, A. G. (2011). The dating and interpretation of a Mode 1 site in the Luangwa Valley, Zambia. Journal of Human Evolution, 60(5), 549–570. https://doi.org/10.1016/J.JHEVOL.2010.12.003

Benoit, R., Côté, J., & Mailhot, J. (1989). Inclusion of a TKE Boundary Layer Parameterization in the Canadian Regional Finite-Element Model. Monthly Weather Review, 117(8), 1726–1750. https://doi.org/10.1175/1520-0493(1989)117

Berger, A. (1978). Long-Term Variations of Daily Insolation and Quaternary Climatic Changes. Journal of the Atmospheric Sciences, 35(12), 2362–2367. https://doi.org/10.1175/1520-0469(1978)035<2362:LTVODI>2.0.CO;2

Blome, M. W., Cohen, A. S., Tryon, C. A., Brooks, A. S., & Russell, J. (2012). The environmental context for the origins of modern human diversity: A synthesis of regional variability in African climate 150,000–30,000 years ago. Journal of Human Evolution, 62(5), 563–592. https://doi.org/10.1016/J.JHEVOL.2012.01.011

Burke, A., Bisson, M., Schilt, F., Tolan, S., Museba, J., Drapeau, M. S. M., et al. (2023). The archaeological potential of the northern Luangwa Valley, Zambia: The Luwumbu basin. PLOS ONE, 18(3), e0269209. https://doi.org/10.1371/JOURNAL.PONE.0269209

Burke, Ariane, Peros, M. C., Wren, C. D., Pausata, F. S. R., Riel-Salvatore, J., Moine, O., et al. (2021). The archaeology of climate change: The case for cultural diversity. Proceedings of the National Academy of Sciences of the United States of America, 118(30). https://doi.org/10.1073/pnas.2108537118

Burrough, S. L., Thomas, D. S. G., & Barham, L. S. (2019). Implications of a new chronology for the interpretation of the Middle and Later Stone Age of the upper Zambezi Valley. Journal of Archaeological Science: Reports, 23, 376–389. https://doi.org/10.1016/J.JASREP.2018.10.016

Castañeda, I. S., Mulitza, S., Schefuss, E., Lopes dos Santos, R. A., Sinninghe Damsté, J. S., & Schouten, S. (2009). Wet phases in the Sahara/Sahel region and human migration patterns in North Africa. Proceedings of the National Academy of Sciences of the United States of America, 106(48), 20159–63. https://doi.org/10.1073/pnas.0905771106

Colton, D., Whitfield, E., Plater, A. J., Duller, G. A. T., Jain, M., & Barham, L. (2021). New geomorphological and archaeological evidence for drainage evolution in the

Luangwa Valley (Zambia) during the Late Pleistocene. Geomorphology, 392, 107923. https://doi.org/10.1016/J.GEOMORPH.2021.107923

Daly, M. C., Green, P., Watts, A. B., Davies, O., Chibesakunda, F., & Walker, R. (2020). Tectonics and Landscape of the Central African Plateau and their Implications for a Propagating Southwestern Rift in Africa. Geochemistry, Geophysics, Geosystems, 21(6), e2019GC008746. https://doi.org/10.1029/2019GC008746

Dandoy, S., Pausata, F. S. R., Camargo, S. J., Laprise, R., Winger, K., & Emanuel, K. (2021). Atlantic hurricane response to Saharan greening and reduced dust emissions during the mid-Holocene. Climate of the Past, 17(2), 675–701. https://doi.org/10.5194/CP-17-675-2021

Delage, Y. (1997). Parameterising Sub-Grid Scale Vertical Transport in Atmospheric Models Under Statically Stable Conditions. Boundary-Layer Meteorology, 82(1), 23–48. https://doi.org/10.1023/A:1000132524077

Delage, Y., & Girard, C. (1992). Stability functions correct at the free convection limit and consistent for for both the surface and Ekman layers. Boundary-Layer Meteorology, 58(1–2), 19–31. https://doi.org/10.1007/BF00120749/METRICS

deMenocal, P., Ortiz, J., Guilderson, T., Adkins, J., Sarnthein, M., Baker, L., & Yarusinsky, M. (2000). Abrupt onset and termination of the African Humid Period: Quaternary Science Reviews, 19(1–5), 347–361. https://doi.org/10.1016/S0277-3791(99)00081-5

deMenocal, P. B., & Tierney, J. E. (2012). Green Sahara: African Humid Periods Paced by Earth's Orbital Changes. Nature Education Knowledge, 3(10).

Drake, N. A., Blench, R. M., Armitage, S. J., Bristow, C. S., & White, K. H. (2011). Ancient watercourses and biogeography of the Sahara explain the peopling of the desert. Proceedings of the National Academy of Sciences of the United States of America, 108(2), 458–62. https://doi.org/10.1073/pnas.1012231108

Fauchereau, N., Trzaska, S., Rouault, M., & Richard, Y. (2003). Rainfall variability and changes in Southern Africa during the 20th century in the global warming context. Natural Hazards, 29(2), 139–154. https://doi.org/10.1023/A:1023630924100/METRICS

Gaetani, M., Messori, G., Zhang, Q., Flamant, C., & Pausata, F. S. R. (2017). Understanding the mechanisms behind the northward extension of the West African Monsoon during the mid-Holocene. Journal of Climate, 30(19). https://doi.org/10.1175/JCLI-D-16-0299.1

Gasse, F. (2000). Hydrological changes in the African tropics since the Last Glacial Maximum. Quaternary Science Reviews, 19(1–5), 189–211. https://doi.org/10.1016/S0277-3791(99)00061-X

Gasse, F., Téhet, R., Durand, A., Gibert, E., & Fontes, J. C. (1990). The arid–humid transition in the Sahara and the Sahel during the last deglaciation. Nature 1990 346:6280, 346(6280), 141–146. https://doi.org/10.1038/346141a0

Girard, C., Plante, A., Desgagné, M., Mctaggart-Cowan, R., Côté, J., Charron, M., et al. (2014). Staggered Vertical Discretization of the Canadian Environmental Multiscale (GEM) Model Using a Coordinate of the Log-Hydrostatic-Pressure Type. Monthly Weather Review, 142(3), 1183–1196. https://doi.org/10.1175/MWR-D-13-00255.1

Hély, C., Lézine, A.-M., & contributors, A. (2014). Holocene changes in African vegetation: tradeoff between climate and water availability. Climate of the Past, 10(2), 681–686. https://doi.org/10.5194/cp-10-681-2014

Hoelzmann, P., Jolly, D., Harrison, S. P., Laarif, F., Bonnefille, R., & Pachur, H.-J. (1998). Mid-Holocene land-surface conditions in northern Africa and the Arabian Peninsula: A data set for the analysis of biogeophysical feedbacks in the climate system. Global Biogeochemical Cycles, 12(1), 35–51. https://doi.org/10.1029/97GB02733

Hublin, J. J., Ben-Ncer, A., Bailey, S. E., Freidline, S. E., Neubauer, S., Skinner, M. M., et al. (2017). New fossils from Jebel Irhoud, Morocco and the pan-African origin of Homo sapiens. Nature 2017 546:7657, 546(7657), 289–292. https://doi.org/10.1038/nature22336

Kain, J. S., & Fritsch, J. M. (1990). A One-Dimensional Entraining/Detraining Plume Model and Its Application in Convective Parameterization. Journal of the Atmospheric Sciences, 47(23), 2784–2802. https://doi.org/10.1175/1520-0469(1990)047

Klein, R. G., & Richard Klein, C. G. (2019). Population structure and the evolution of Homo sapiens in Africa. Evolutionary Anthropology: Issues, News, and Reviews, 28(4), 179–188. https://doi.org/10.1002/EVAN.21788

Kuo, H. L. (1965). On Formation and Intensification of Tropical Cyclones Through Latent Heat Release by Cumulus Convection. Journal of the Atmospheric Sciences, 22(1), 40–63. https://doi.org/10.1175/1520-0469(1965)022

Kutzbach, J. E., & Liu, Z. (1997). Response of the African Monsoon to Orbital Forcing and Ocean Feedbacks in the Middle Holocene. Science, 278(5337), 440–443. https://doi.org/10.1126/science.278.5337.440

Kutzbach, J E. (1981). Monsoon Climate of the Early Holocene: Climate Experiment with the Earth's Orbital Parameters for 9000 Years Ago. Science (New York, N.Y.), 214(4516), 59–61. https://doi.org/10.1126/science.214.4516.59

Kutzbach, John E., Guan, J., He, F., Cohen, A. S., Orland, I. J., & Chen, G. (2020). African climate response to orbital and glacial forcing in 140,000-y simulation with implications for early modern human environments. Proceedings of the National Academy of Sciences of the United States of America, 117(5), 2255–2264. https://doi.org/10.1073/PNAS.1917673117/SUPPL_FILE/PNAS.1917673117.SAPP.PDF

Larrasoaña, J. C., Roberts, A. P., & Rohling, E. J. (2013). Dynamics of Green Sahara Periods and Their Role in Hominin Evolution. PLoS ONE, 8(10), e76514. https://doi.org/10.1371/journal.pone.0076514

Li, J., & Barker, H. W. (2005). A Radiation Algorithm with Correlated-k Distribution. Part I: Local Thermal Equilibrium. Journal of the Atmospheric Sciences, 62(2), 286–309. https://doi.org/10.1175/JAS-3396.1

Manhique, A. J., Reason, C. J. C., Silinto, B., Zucula, J., Raiva, I., Congolo, F., & Mavume, A. F. (2015). Extreme rainfall and floods in southern Africa in January 2013 and associated circulation patterns. Natural Hazards, 77(2), 679–691. https://doi.org/10.1007/S11069-015-1616-Y/FIGURES/9

Martynov, A., Sushama, L., Laprise, R., Winger, K., & Dugas, B. (2012). Interactive lakes in the Canadian Regional Climate Model, version 5: the role of lakes in the regional climate of North America. New Pub: Stockholm Uni Press, 64(1). https://doi.org/10.3402/TELLUSA.V64I0.16226

Mason, S. J., & Jury, M. R. (1997). Climatic variability and change over southern Africa: a reflection on underlying processes. Http://Dx.Doi.Org/10.1177/030913339702100103, 21(1), 23–50. https://doi.org/10.1177/030913339702100103

Masson, V., Champeaux, J.-L., Chauvin, F., Meriguet, C., Lacaze, R., Masson, V., et al. (2003). A Global Database of Land Surface Parameters at 1-km Resolution in Meteorological and Climate Models. Journal of Climate, 16(9), 1261–1282. https://doi.org/10.1175/1520-0442-16.9.1261

McFarlane, & A., N. (1987). The Effect of Orographically Excited Gravity Wave Drag on the General Circulation of the Lower Stratosphere and Troposphere. Journal of the Atmospheric Sciences, 44(14), 1775–1800. https://doi.org/10.1175/1520-0469(1987)044

McTaggart-Cowan, R., Vaillancourt, P. A., Zadra, A., Chamberland, S., Charron, M., Corvec, S., et al. (2019). Modernization of Atmospheric Physics Parameterization

in Canadian NWP. Journal of Advances in Modeling Earth Systems, 11(11), 3593–3635. https://doi.org/10.1029/2019MS001781

Nicholson, S. E. (2019). A Review of Climate Dynamics and Climate Variability in Eastern Africa. The Limnology, Climatology and Paleoclimatology of the East African Lakes, 25–56. https://doi.org/10.1201/9780203748978-2

Osborne, A. H., Vance, D., Rohling, E. J., Barton, N., Rogerson, M., & Fello, N. (2008). A humid corridor across the Sahara for the migration of early modern humans out of Africa 120,000 years ago. Proceedings of the National Academy of Sciences of the United States of America, 105(43), 16444–7. https://doi.org/10.1073/pnas.0804472105

Otto-Bliesner, B. L., Braconnot, P., Harrison, S. P., Lunt, D. J., Abe-Ouchi, A., Albani, S., et al. (2016). The PMIP4 contribution to CMIP6. Part 2: Two Interglacials, Scientific Objective and Experimental Design for Holocene and Last Interglacial Simulations. Geoscientific Model Development, 10, 3979–4003. https://doi.org/10.5194/gmd-2016-279

Pausata, F.S.R., Zhang, Q., Muschitiello, F., Lu, Z., Chafik, L., Niedermeyer, E. M., et al. (2017). Greening of the Sahara suppressed ENSO activity during the mid-Holocene. Nature Communications, 8. https://doi.org/10.1038/ncomms16020

Pausata, F.S.R., Emanuel, K. A., Chiacchio, M., Diro, G. T., Zhang, Q., Sushama, L., et al. (2017). Tropical cyclone activity enhanced by Sahara greening and reduced dust emissions during the African Humid Period. Proceedings of the National Academy of Sciences of the United States of America, 114(24), 6221–6226. https://doi.org/10.1073/pnas.1619111114

Pausata, F.S.R., Messori, G., Yun, J., Jalihal, C. A., Bollasina, M. A., & Marchitto, T. M. (2021). The remote response of the South Asian Monsoon to reduced dust

emissions and Sahara greening during the middle Holocene. Climate of the Past, 17(3), 1243–1271. https://doi.org/10.5194/CP-17-1243-2021

Pausata, Francesco S.R., Messori, G., & Zhang, Q. (2016). Impacts of dust reduction on the northward expansion of the African monsoon during the Green Sahara period. Earth and Planetary Science Letters, 434, 298–307. https://doi.org/10.1016/j.epsl.2015.11.049

Piao, J., Chen, W., Wang, L., Pausata, F. S. R., & Zhang, Q. (2020). Northward extension of the East Asian summer monsoon during the mid-Holocene. Global and Planetary Change, 184, 103046. https://doi.org/10.1016/J.GLOPLACHA.2019.103046

Reynolds, S. C. (2015). The role of landscapes in shaping hominin habitats in Africa. In A. R. Sankhyan (Ed.), Recent Discoveries and Perspectives in Human Evolution (pp. 68–76). Oxford, England: British Archaeological Reports. Retrieved from https://staffprofiles.bournemouth.ac.uk/display/chapter/210794

Richard, Y., Fauchereau, N., Poccard, I., Rouault, M., & Trzaska, S. (2001). 20th century droughts in southern Africa: spatial and temporal variability, teleconnections with oceanic and atmospheric conditions. International Journal of Climatology, 21(7), 873–885. https://doi.org/10.1002/JOC.656

Richter, D., Grün, R., Joannes-Boyau, R., Steele, T. E., Amani, F., Rué, M., et al. (2017). The age of the hominin fossils from Jebel Irhoud, Morocco, and the origins of the Middle Stone Age. Nature, 546(7657), 293–296. https://doi.org/10.1038/nature22335

Scerri, E. M. L. (2017). The North African Middle Stone Age and its place in recent human evolution. Evolutionary Anthropology: Issues, News, and Reviews, 26(3), 119–135. https://doi.org/10.1002/EVAN.21527

Smith, J. R. (2012). Spatial and Temporal Variation in the Nature of Pleistocene Pluvial Phase Environments Across North Africa. Vertebrate Paleobiology and

Paleoanthropology, (9789400729285), 35–47. https://doi.org/10.1007/978-94-007-2929-2_3/COVER

Stringer, C., & Galway-Witham, J. (2017). On the origin of our species. Nature 2017 546:7657, 546(7657), 212–214. https://doi.org/10.1038/546212a

Sun, W., Wang, B., Zhang, Q., Pausata, F. S. R., Chen, D., Lu, G., et al. (2019). Northern Hemisphere Land Monsoon Precipitation Increased by the Green Sahara During Middle Holocene. Geophysical Research Letters, 46(16), 9870–9879. https://doi.org/10.1029/2019GL082116

Sundquist, H., Berge, E., & Kristjansson, J. E. (1989). Condensation and cloud parameterization studies with a mesoscale numerical prediction model. Mon.Wea.Rev., 117, 1641–1657.

Szabo, B. J., Haynes, C. V., & Maxwell, T. A. (1995). Ages of Quaternary pluvial episodes determined by uranium-series and radiocarbon dating of lacustrine deposits of Eastern Sahara. Palaeogeography, Palaeoclimatology, Palaeoecology, 113(2–4), 227–242. https://doi.org/10.1016/0031-0182(95)00052-N

Taylor, K. E., Stouffer, R. J., & Meehl, G. A. (2009). A Summary of the CMIP5 Experiment Design. Retrieved from http://cmip-pcmdi.llnl.gov/cmip5/docs/Taylor_CMIP5_design.pdf

Tierney, J. E., Pausata, F. S. R., & De Menocal, P. B. (2017). Rainfall regimes of the Green Sahara. Science Advances, 3(1). https://doi.org/10.1126/sciadv.1601503

Timmermann, A., & Friedrich, T. (2016). Late Pleistocene climate drivers of early human migration. Nature 2016 538:7623, 538(7623), 92–95. https://doi.org/10.1038/nature19365

Verseghy, D. L. (2000). The Canadian land surface scheme (CLASS): Its history and future. Atmosphere-Ocean, 38(1), 1–13. https://doi.org/10.1080/07055900.2000.9649637

Verseghy, D. L. (2010). The Canadian land surface scheme (CLASS): Its history and future. Http://Dx.Doi.Org/10.1080/07055900.2000.9649637, 38(1), 1–13. https://doi.org/10.1080/07055900.2000.9649637

Vogel, C. H., & Drummond, J. H. (1993). Drought and Economic Distress: South Africa in the 1800s. GeoJournal, 30,(1), 93–98. https://doi.org/10.2307/204770

Wilcoxon, F. (1945). Individual Comparisons by Ranking Methods. Biometrics Bulletin, 1(6), 80. https://doi.org/10.2307/3001968

Wilkins, J. (2021). Homo sapiens origins and evolution in the Kalahari Basin, southern Africa. Evolutionary Anthropology: Issues, News, and Reviews, 30(5), 327–344. https://doi.org/10.1002/EVAN.21914

Yu, G., & Harrison, S. P. (1996). An evaluation of the simulated water balance of Eurasia and northern Africa at 6000 y BP using lake status data. Climate Dynamics, 12(11), 723–735. https://doi.org/10.1007/S003820050139/METRICS

Yuen, K. K., & Dixon, W. J. (1973). The approximate behaviour and performance of the two sample trimmed t. Biometrika, 60(2), 369–374. https://doi.org/10.2307/2334550

Zadra, A., Roch, M., Laroche, S., & Charron, M. (2010). The subgrid-scale orographic blocking parametrization of the GEM Model. Atmosphere-Ocean, 41(2), 155–170. https://doi.org/10.3137/AO.410204

Zhang, X., Alexander, L., Hegerl, G. C., Jones, P., Tank, A. K., Peterson, T. C., et al. (2011). Indices for monitoring changes in extremes based on daily temperature and precipitation data. Wiley Interdisciplinary Reviews: Climate Change, 2(6), 851–870. https://doi.org/10.1002/WCC.147